*J. Fluid Mech.* (1987), *vol.* 181, *pp.* 485–517
*Printed in Great Britain*



# Generation of Tollmien–Schlichting waves on interactive marginally separated flows

By M. E. GOLDSTEIN, S. J. LEIB
Lewis Research Center, Cleveland, OH 44135, USA

AND S. J. COWLEY
Imperial College of Science and Technology, Department of Mathematics, London SW7 2BZ, UK

(Received 7 July 1986)

This paper is concerned with the interaction of very long-wavelength free-stream disturbances with the small but abrupt changes in the mean flow that occur near the minimum-skin-friction point in an interactive marginally separated boundary layer. We choose the source frequency so that the eigensolutions with that frequency have an 'interactive' structure in the region of marginal separation. The eigensolution wavelength scale must then differ from the lengthscale of the marginal separation and a composite expansion technique has to be used to obtain the solution.

The initial instability wave amplitude turns out to be exponentially small, but eventually dominates the original disturbance owing to its exponential growth. It then begins to decay but ultimately turns into a standard spatially growing Tollmien–Schlichting wave much further downstream.

## 1. Introduction

There is now considerable interest in understanding how free-stream disturbances generate Tollmien–Schlichting waves in laminar boundary layers. The relevant experiments are usually carried out by minimizing background disturbances and imposing a controlled excitation of a single frequency, say $\omega$, on the flow. The Mach numbers are usually quite small so that the wavelengths or spatial scales of the free-stream disturbances tend to be much larger than the Tollmien–Schlichting wavelength, especially for acoustic disturbances (which happen to be very effective Tollmien–Schlichting-wave generators). The key to understanding these so-called 'receptivity' experiments (Morkovin 1969) lies in understanding how the very long wavelengths of the free-stream disturbances are reduced to the very short Tollmien–Schlichting wavelengths (Reshotko 1976). It is now clear that this can usually be attributed to non-uniform or non-parallel mean flow effects which arise from (i) the slow, viscous boundary-layer growth, (ii) small but sudden changes in surface geometry or (iii) relatively slow variations in surface static pressure.

Case (i) was studied analytically by Goldstein (1983) and Goldstein, Sockol & Sanz (1983), and numerically by Murdock (1980). Goldstein (1983) showed that the Tollmien–Schlichting waves develop out of the so-called 'Lam & Rott' (1960) asymptotic eigensolutions (see also Ackerberg & Phillips 1972). These are generated near the leading edge, where the unsteady motion is governed by the unsteady boundary-layer equation and is therefore influenced by non-parallel mean flow effects

to lowest order of approximation (but is unaffected by cross-stream pressure fluctuations).

Case (ii) was studied by Goldstein (1985), and independently by Ruban (1985). The sudden geometry change can now introduce a short streamwise lengthscale that can scatter the long-wavelength free-stream disturbances directly into the short Tollmien–Schlichting waves.

Case (iii) is more interesting in that the small lengthscale is not externally imposed but is produced by the mean flow itself. It occurs naturally at the minimum-skin-friction point when the boundary layer is close enough to separation, and the small lengthscale turns out to be of the order of the scaled skin friction multiplied by the downstream distance to that point.

Ruban (1982*a*) and Stewartson, Smith & Kaups (1982) independently showed that the steady-boundary-layer flow becomes interactive when the scaled skin friction is reduced to $O(R^{-\frac{1}{8}})$, where $R$ denotes the Reynolds number based on the downstream distance to the minimum-skin-friction point, and that separation can be expected when the skin friction is smaller than this. This then sets a lower limit to the streamwise lengthscales that can be achieved in such flows.

Ruban (1982*a*) and Stewartson *et al.* (1982) emphasized the 'marginal separation' that occurs near the leading edge of thin bodies close to their critical angles of attack (for leading-edge stall), but the same type of interaction is likely to occur in other flows. The resulting interactive marginally separated flow has a triple-layer structure, which is somewhat different from the conventional 'triple deck'. It is important to notice that such interactions occur even when there is no backflow.

It is natural to assume that the steady and unsteady flow have the same streamwise lengthscale, and to adjust the externally imposed source frequency so that the temporal, convective, and viscous effects are all of the same order in an unsteady viscous wall layer. But it then turns out to be impossible to specifically identify spatially growing Tollmien–Schlichting waves produced in the resulting unsteady flow. We therefore decided to make the unsteady-flow lengthscale somewhat shorter than that of the steady flow and thereby allow the unsteady flow to contain normal modes with wavelengths that are shorter than the streamwise mean flow scale.

The steady marginally separated boundary layer is able to support various types of eigenmodes (summarized in Appendix C). We scaled the 'source frequency' to produce the best coupling between the mean flow and a certain eigenmode which was found to exhibit spatial growth within the region of marginally separated flow itself. This wave eventually begins to decay and ultimately becomes non-interactive† in a somewhat larger 'outer' region, where the steady marginal separation is non-interactive. The decaying mode then evolves into a conventional spatially growing Tollmien–Schlichting wave on a much longer streamwise lengthscale.

There is an important aspect of the analysis that arises from the mismatch of lengthscales of the initial steady and unsteady flows. The mismatch causes the initial instability wave amplitudes to be exponentially small relative to the free-stream disturbance amplitudes (i.e. $O(\mathrm{e}^{-r})$ where $r$ is the lengthscale of steady flow/lengthscale of unsteady flow, and is $O(R^{\frac{3}{35}})$ for the disturbance frequency being considered herein). A 'straightforward' asymptotic solution that did not account for causality at the outset would miss these crucially important terms, which grow exponentially and very quickly dominate the original disturbance. However the steady-state causal solution must, in principle, be thought of as the long-time limit of the solution to

† Here we mean non-interactive in the 'triple-deck' sense.

an initial-value problem. The asymptotic solution to this latter problem turns out to be non-uniformly valid in frequency space, when scaled on the source frequency, with the result that the steady-state limit fails to exist. But, the steady-state limit does exist when the solution is first rendered uniformly valid in frequency space (e.g. by means of a composite expansion) and the instability wave then appears naturally as part of this solution.

The structure of the paper is as follows. The theory of interactive marginally separated steady flow is reviewed in §2.1. The unsteady motion resulting from the interaction of a small-amplitude harmonic oscillation of the free stream with that flow is analysed in §2.2. We show that the latter is 'convectively' unstable so that the steady-state causal solution exists in the sense that any unsteady solution satisfying appropriate causal initial conditions becomes time harmonic after a sufficiently long period of time. This solution uniquely determines the amplitude of the instability-wave eigensolution produced by the interaction. Its subsequent downstream evolution is traced out in §3, where we show that the eigensolution begins to decay as the wall shear increases towards an order-one value and that there is an accompanying increase in its wavelength as it evolves into the lowest-order, non-interactive, Lam–Rott asymptotic eigensolution. This latter eigensolution then turns into a spatially growing Tollmien–Schlichting wave by the wavelength-reduction mechanism described by Goldstein (1983), and the formulas given therein can be used to trace the eigensolution's subsequent development.

The effective 'coupling coefficient' and other results are discussed in §4 and some comparisons with experiment are given. Appendix C describes the various types of eigenmodes that can exist in various frequency ranges and also explains how solutions for different ranges of frequencies and values of the minimum wall shear can be obtained as limiting cases of the scaling studied here.

## 2. The inner solution

We consider a two-dimensional incompressible laminar flow of density $\rho$ and kinematic viscosity $\nu$ over a relatively thin two-dimensional body at an angle of attack $\sigma$ close to the critical stall angle $\sigma_c$ as predicted by classical boundary-layer theory. The precise decrement will be specified more completely below. The upstream motion is assumed to consist of a uniform flow with velocity $U_\infty$ plus a small harmonic perturbation of frequency $\omega$ and constant amplitude $u_\infty \ll U_\infty$, so that the unsteady motion can be treated as a linear perturbation of the steady flow.

We introduce orthogonal coordinates $\{x^*, y^*\}$ with $x^*$ tangent to the body surface as shown in figure 1. The steady velocity $\{U, V\}$ and pressure $P$ are assumed to be normalized by $U_e$ and $\rho U_e^2$ respectively, where $U_e$ is the free-stream velocity just outside the boundary layer at the minimum-skin-friction point $x_c^*$, while the unsteady velocity perturbation $\{u, v\}$ and pressure perturbation $p$ are assumed to be normalized by $u_e$ and $\rho u_e U_\infty$, respectively, where $u_e$ denotes the magnitude of the inviscid streamwise velocity fluctuation at $x_c^*$. We let $l$ denote the characteristic distance between the leading edge and $x_c^*$ and require that the Reynolds number $R = U_e l/\nu$ based on this distance be large. ($U_e$ will usually be $O(U_\infty)$ but $l = O(\sigma^2 l_\infty)$, where $l_\infty$ is the streamwise body dimension, for slender bodies at small angle of attack.)

Introducing the scaled coordinates

$$x = \frac{x^*}{l}; \quad y = \frac{y^*}{lR^{-\frac{1}{2}}}, \tag{2.1}$$

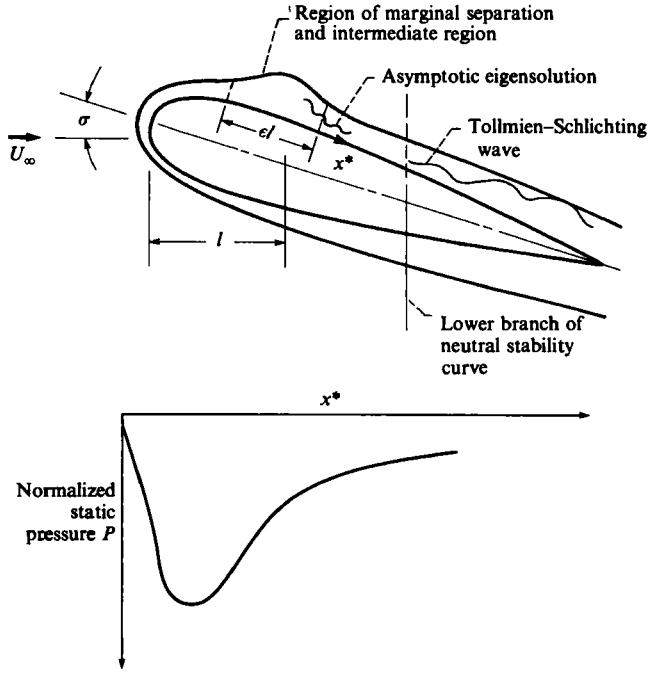


FIGURE 1. Overall flow configuration.

and following Ruban (1982*a*) and Stewartson *et al.* (1982), we suppose that $\sigma$ is close enough to $\sigma_c$ that the normalized wall shear

$$\tau = x^{\frac{1}{2}}\left(\frac{\partial U}{\partial y}\right)_{y=0} \tag{2.2}$$

(where we have introduced the $x^{\frac{1}{2}}$ for convenience in considering the outer scale flow) behaves like

$$\tau \propto [(x-x_c)^2+\gamma(\sigma_c-\sigma)]^{\frac{1}{2}}. \tag{2.3}$$

with $\gamma > 0$ for $x$ near $x_c$. Ruban (1982*a*) and Stewartson *et al.* (1982) showed that the *steady* flow becomes interactive, and exhibits a three-layered structure in the region where

$$x_1 \equiv \frac{x-x_c}{R^{-\frac{1}{8}}} \tag{2.4}$$

is $O(1)$, when the normalized minimum wall shear

$$\tau_{\min} \propto [\gamma(\sigma_c-\sigma)]^{\frac{1}{2}}$$

is $O(R^{-\frac{1}{8}})$. This serves to smooth out the discontinuity in the skin-friction gradient that would otherwise occur in the local boundary-layer solution. This scaling produces the shortest possible streamwise lengthscale that can occur in an attached flow, and is therefore the one of major interest in this work.

The upstream flow will then correspond to Goldstein's (1948) non-singular 'ex-

ceptional case' and the streamwise boundary-layer velocity just upstream of the marginal separation will therefore be of the form

$$U_0 = \tfrac{1}{2}\mu y^2 + \frac{\mu_6 y^6}{6!} + O(y^8) \quad \text{as } y \to 0, \tag{2.5}$$

where the $O(1)$ constant $\mu$ is equal to the normalized static pressure gradient just upstream of the region of marginal separation. Ruban (1982*a*) and Stewartson *et al.* (1982) show that this is consistent with the numerical boundary-layer solutions at the minimum-skin-friction point $x_c$ on slender bodies close to their critical angles of attack $\sigma = \sigma_c$, while the singular general case is not. This suggests that local interactions, of the type being considered herein, will occur in flows where the separation is 'marginal' in the sense that the skin friction vanishes, or better, nearly vanishes at some position but then immediately recovers downstream of that position.

The analysis applies when $\sigma$ is asymptotically close to $\sigma_c$, and it is worth noting that the steady flow remains interactive even when $\sigma < \sigma_c$. Stewartson *et al.* (1982) found that no solution exists above a certain angle of attack $\sigma_{\max}$ and that there are two solutions for the range $\sigma_c < \sigma < \sigma_{\max}$. One of these involves backflow, and (as conjectured by Ryzhov & Smith 1984) may be absolutely as opposed to convectively unstable. It therefore would not be achievable as the steady-state limit of the solution to a well-posed initial-value problem.

### 2.1. *The steady flow*

For convenience, the relevant portion of Ruban's (1982*a*) and Stewartson's *et al.* (1982) analyses are summarized in this section. The asymptotic structure of the flow is illustrated in figure 2. In the 'main deck' where $y = O(1)$ it is of the form

$$U = U_0(y) + R^{-\frac{1}{8}} U_1(x_1, y) + R^{-\frac{2}{8}} U_2(x_1, y) + \ldots, \tag{2.6}$$

$$V = R^{-\frac{1}{8}}[V_1(x_1, y) + R^{-\frac{1}{8}} V_2(x_1, y) + \ldots], \tag{2.7}$$

$$P = P_0 + R^{-\frac{1}{8}}\mu x_1 + R^{-\frac{2}{8}}\frac{\mu_6}{4\mu} x_1^2 + R^{-\frac{1}{2}} P(x_1) + \ldots, \tag{2.8}$$

where $U_0$ is the streamwise velocity of the boundary-layer flow just upstream of the interaction region (and therefore satisfies (2.5)), $P_0$ is the constant static pressure level at the interaction region,

$$U_1 = U_0'(y)\, A(x_1) - x_1 V_0'. \tag{2.9}$$

$$V_1 = -U(y)\, A'(x_1) + V_0(y), \tag{2.10}$$

$$V_0 \equiv -U_0(y) \int_0^y \frac{U_0'' - \mu}{U_0^2}\, \mathrm{d}y, \tag{2.11}$$

and $A$ and $P$ are related, via the 'upper-deck' solution, by the Cauchy integral

$$A'(x_1) = \frac{1}{\pi} \bar{\int}_{-\infty}^{\infty} \frac{P(\tilde{x}_1)}{\tilde{x}_1 - x_1}\, \mathrm{d}\tilde{x}_1, \tag{2.12}$$

where the bar indicates that the Cauchy principal value of the integral is to be taken.

The steady flow in the lower deck, where

$$y_1 \equiv \frac{y}{R^{-\frac{1}{10}}} \tag{2.13}$$

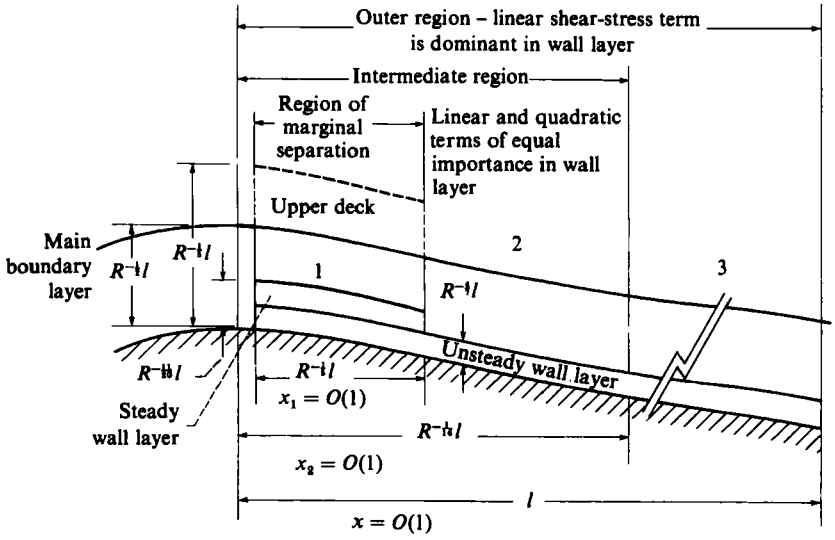


FIGURE 2. Boundary-layer flow structure.

is $O(1)$, has an expansion of the form

$$U = R^{-\frac{1}{10}}\tfrac{1}{2}\mu y_1^2 + \mu R^{-\frac{1}{4}} A y_1 + R^{-\frac{3}{10}}\left[\frac{\mu_6}{6!}y_1^6 + \frac{\mu_6}{4\mu}x_1 y_1^2\right] + R^{-\frac{3}{5}}\frac{\partial \Psi}{\partial y_1} + \ldots, \tag{2.14}$$

$$V = -\tfrac{1}{2}\mu R^{-\frac{3}{5}} A' y_1^2 - R^{-\frac{13}{10}}\frac{\mu_6}{12\mu}y_1^3 - R^{-\frac{3}{4}}\frac{\partial \Psi}{\partial x_1} + \ldots, \tag{2.15}$$

$$P = P_0 + R^{-\frac{1}{5}}\mu x_1 + R^{-\frac{3}{5}}\frac{\mu_6}{4\mu}x_1^2 + R^{-\frac{1}{2}}P(x_1) + \ldots, \tag{2.16}$$

where $\Psi$ is determined by

$$\tfrac{1}{2}\mu^2 A A' y_1^2 + P' = \frac{\partial^3 \Psi}{\partial y_1^3} - \tfrac{1}{2}\mu y_1^2 \frac{\partial^2 \Psi}{\partial y_1 \partial x_1} + \mu y_1 \frac{\partial \Psi}{\partial x_1}, \tag{2.17}$$

$$\Psi = \frac{\partial \Psi}{\partial y_1} = 0 \quad \text{for } y_1 = 0, \tag{2.18}$$

and

$$|\Psi| \leqslant O(y_1^9) \quad \text{as } y_1 \to \infty. \tag{2.19}$$

If $\Psi$ is to match with the main deck, the solvability of this system requires that $A$ and $P$ be related by

$$\tfrac{1}{2}\mu^2 A A' - \tfrac{1}{2}\lambda_0'^2(x_1 - x_0) + C_0 \int_{-\infty}^{x_1} \frac{p'' \mathrm{d}\tilde{x}_1}{(x_1 - \tilde{x}_1)^{\frac{1}{2}}} = 0, \tag{2.20}$$

where

$$C_0 \equiv \frac{(\frac{1}{2}\mu)^{\frac{1}{2}}(-\frac{1}{4})!}{(-\frac{3}{4})!}, \tag{2.21}$$

the constant $\lambda_0'$ is obtained from the matching condition with the oncoming boundary layer

$$A \sim \frac{\lambda_0'}{\mu}(x_1^2 + (\tau_0/\lambda_0')^2)^{\frac{1}{2}} \quad \text{as } x_1 \to \pm\infty, \tag{2.22}$$

$\tau_0$ is a constant defined more precisely in (2.89) below, and $x_0$ represents an unimportant shift in origin. $P$ can be eliminated between (2.12) and (2.20) to obtain a single nonlinear integral–differential equation for $A$.

### 2.2. *The unsteady flow*

We suppose that the time $t$ has been normalized by $l/U_e$ and introduce the Strouhal number $S$ by

$$S \equiv \frac{\omega l}{U_e}. \tag{2.23}$$

Our steady flow has the shortest possible streamwise lengthscale and, as indicated in §1, we originally assumed that the unsteady flow had the same streamwise lengthscale. We then scaled $S$ so that the temporal, convective and viscous effects were all of the same order in a thin viscous wall layer. But the resulting unsteady flow turned out to be non-interactive (in the 'triple-deck' sense) and, even more importantly, the spatially growing Tollmien–Schlichting wave could not evolve from any of the normal modes generated by the interaction (see §4 below).

We therefore scale $S$ so that there is a corresponding eigenmode of the steady marginally separated boundary layer with streamwise lengthscale, say $l\delta$, that is somewhat shorter than that of the mean flow, and specifically require that it be short enough to make the resulting disturbance interactive and fully unsteady in its lower deck (see the remarks following (2.46)).

To this end, we notice that the continuity equation requires that the normalized transverse velocity fluctuation $v$ be $O(A^+/\delta R^{\frac{1}{8}})$ in the main deck where $y = O(1)$, when the normalized streamwise velocity fluctuation $u$ is $O(A^+)$ there. The former forces a normalized pressure fluctuation $p$ of the same order of magnitude in the upper deck, and the latter then remains unchanged across the entire boundary layer.

The velocity fluctuation in the main deck forces an $O(\epsilon A^+)$ streamwise velocity fluctuation in the lower deck, where $y = O(\epsilon)$ say, and the normalized mean velocity is $O(\epsilon^2)$ there (cf. (2.5)). The temporal, convective, pressure gradient and viscous terms in the linearized unsteady streamwise momentum equation are therefore $O(S\epsilon A^+)$, $O(\epsilon^3 A^+/\delta)$, $O(A^+/\delta^2 R^{\frac{1}{8}})$, and $O(A^+/\epsilon)$ respectively, in this region. The fully unsteady triple-deck interaction occurs when they are all of equal magnitude, which implies that

$$\epsilon \equiv R^{-\frac{1}{11}}, \tag{2.24}$$

and that the appropriate $O(1)$ scaled Strouhal number is

$$S_0 \equiv \epsilon^2 S. \tag{2.25}$$

The relevant streamwise lengthscale is then $\delta = \epsilon^4$, which corresponds to the scaling

$$X \equiv \frac{x - x_c}{\epsilon^4}. \tag{2.26}$$

The imposed disturbance is assumed to be small enough that the unsteady problem is completely linear. Then upstream of the interaction region, where the mean flow changes on the scale $l$ in the streamwise direction, the relatively high frequency of the disturbances ensures that the unsteady flow will have harmonic time dependence and vary only slowly in the streamwise direction. The leading-order unsteady flow is therefore given by a Stokes-layer solution with a slowly varying amplitude

(Lighthill 1954). Then, with our scaling, the solution just upstream of the interaction can be written as

$$u = u_0\,\mathrm{e}^{-\mathrm{i}St}, \tag{2.27}$$

$$v = 0,$$

$$p = \mathrm{i}S(x-x_c)\,\mathrm{e}^{-\mathrm{i}St}, \tag{2.28}$$

where we have put $$u_0 \equiv 1-\mathrm{e}^{(\mathrm{i}^3S)^{\frac{1}{2}}y} = 1-\mathrm{e}^{(\mathrm{i}^3S_0)^{\frac{1}{2}}Y}, \tag{2.29}$$

and the scaled transverse coordinate

$$Y \equiv \frac{y}{\epsilon} \tag{2.30}$$

is order one in the Stokes layer.

The solution to the relevant initial-value problem in the marginally separated region can be written as an inverse Laplace transform to obtain

$$u = u_0\,\mathrm{e}^{-\mathrm{i}St} + \frac{1}{2\pi\mathrm{i}}\int_{-\infty+\mathrm{i}C}^{\infty+\mathrm{i}C}\frac{\mathrm{e}^{-\mathrm{i}\mathscr{S}t}}{\mathscr{S}-S}\tilde{u}_{\mathscr{S}}(x_1, Y)\,\mathrm{d}\mathscr{S}, \tag{2.31}$$

$$v = \frac{1}{2\pi\mathrm{i}}\int_{-\infty+\mathrm{i}C}^{\infty+\mathrm{i}C}\frac{\mathrm{e}^{-\mathrm{i}\mathscr{S}t}}{\mathscr{S}-S}\tilde{v}_{\mathscr{S}}(x_1, Y)\,\mathrm{d}\mathscr{S}, \tag{2.32}$$

$$p = \mathrm{i}S(x-x_c)\,\mathrm{e}^{-\mathrm{i}St} + \frac{1}{2\pi\mathrm{i}}\int_{-\infty+\mathrm{i}C}^{\infty+\mathrm{i}C}\frac{\mathrm{e}^{-\mathrm{i}\mathscr{S}t}}{\mathscr{S}-S}\tilde{p}_{\mathscr{S}}(x_1)\,\mathrm{d}\mathscr{S}, \tag{2.33}$$

where $C \geqslant 0$, and $\tilde{u}_{\mathscr{S}}$, $\tilde{v}_{\mathscr{S}}$, and $\tilde{p}_{\mathscr{S}}$ satisfy the linearized unsteady boundary-layer equations

$$-\mathrm{i}\mathscr{S}\tilde{u}_{\mathscr{S}} + R_3^{\frac{1}{3}}(U\tilde{u}_{\mathscr{S}x_1} + \tilde{u}_{\mathscr{S}}U_{x_1}) + R_3^{\frac{1}{3}}(\tilde{v}_{\mathscr{S}}U_y + V\tilde{u}_{\mathscr{S}y}) + R_3^{\frac{1}{3}}\tilde{p}_{\mathscr{S}x_1} - \tilde{u}_{\mathscr{S}yy} = R_3^{\frac{1}{3}}U_{x_1}u_0 + R_7^{\frac{4}{7}}V\frac{\mathrm{d}u_0}{\mathrm{d}Y}, \tag{2.34}$$

$$R_3^{\frac{1}{3}}\tilde{u}_{\mathscr{S}x_1} + \tilde{v}_{\mathscr{S}y}R_2^{\frac{1}{2}} = 0, \tag{2.35}$$

to the appropriate level of approximation. We have set the unimportant initial conditions to zero and, again to lowest approximation, we must require that

$$\tilde{u}_{\mathscr{S}} \to 0 \quad \text{as } y \to \infty \tag{2.36}$$

and

$$\tilde{u}_{\mathscr{S}} = \tilde{v}_{\mathscr{S}} = 0 \quad \text{at } y = 0. \tag{2.37}$$

The steady-state 'causal' solution exists only when the integration contour in (2.31)–(2.33) can be continuously deformed onto the real axis without crossing a singularity of the integrand (Briggs 1964; Bers 1975), in which case that solution is given by $u = \mathrm{e}^{-\mathrm{i}St}(u_0+\tilde{u}_S)$, etc., where $\tilde{u}_S \equiv \tilde{u}_{\mathscr{S}}|_{\mathscr{S}=S}$.

We anticipate that the unsteady solution will exhibit the usual multilayered structure.

(i) In the main boundary layer, where $y = O(1)$, it will be of the form

$$\tilde{u}_{\mathscr{S}} = \epsilon^2 U_0' a(X, x_1, \epsilon) + o(\epsilon^{\frac{16}{5}}), \tag{2.38}$$

$$\tilde{v}_{\mathscr{S}} = -\epsilon^5 U_0\frac{\mathrm{d}a(X, x_1, \epsilon)}{\mathrm{d}X} + o(\epsilon^{\frac{16}{5}}), \tag{2.39}$$

$$\tilde{p}_{\mathscr{S}} = \epsilon^5 p_0(X, x_1, \epsilon) + o(\epsilon^{\frac{21}{5}}), \tag{2.40}$$

where the displacement $a$ and pressure $p_0$ are to be determined.

(ii) When

$$\mathscr{S}_0 \equiv \epsilon^2 \mathscr{S} \tag{2.41}$$

is order one, there is no need to explicitly distinguish the $y_1 = O(1)$ region, i.e. the steady lower deck, at the present level of approximation; (2.38)–(2.40) remain valid there. But closer to wall, where $Y = O(1)$, we expect the solution to be of the form

$$\tilde{u}_{\mathscr{S}} = \epsilon^3 u_1(X, Y, x_1, \epsilon) + o(\epsilon^{\frac{21}{5}}), \tag{2.42}$$

$$\tilde{v}_{\mathscr{S}} = \epsilon^7 v_1(X, Y, x_1, \epsilon) + o(\epsilon^{\frac{33}{5}}), \tag{2.43}$$

$$\tilde{p}_{\mathscr{S}} = \epsilon^5 p_0(X, x_1, \epsilon) + o(\epsilon^{\frac{31}{5}}). \tag{2.44}$$

(iii) Finally $a$ and $p_0$ are related by the usual subsonic upper-deck displacement law

$$\frac{\mathrm{d}a}{\mathrm{d}X} = \frac{1}{\pi} \int_{-\infty}^{\infty} \frac{p_0(\bar{X})}{\bar{X} - X} \mathrm{d}\bar{X}. \tag{2.45}$$

Substituting these, along with (2.13)–(2.16), into (2.34) and (2.35), we find that $u_1$ and $v_1$ satisfy

$$-\mathrm{i}\mathscr{S}_0 u_1 + \tfrac{1}{2}\mu Y^2 \frac{\partial u_1}{\partial X} + \mu Y v_1 - \frac{\partial^2 u_1}{\partial Y^2} = -\frac{\mathrm{d}p_0}{\mathrm{d}X} - \mu A' Y \left(1 - \tfrac{1}{2} Y \frac{\partial}{\partial Y}\right) u_0, \tag{2.46}$$

$$\frac{\partial u_1}{\partial X} + \frac{\partial v_1}{\partial Y} = 0, \tag{2.47}$$

where the prime on the $A$ still denotes differentiation with respect to the slow streamwise variable $x_1$.

It is important to notice that we have explicitly introduced the short streamwise variable $X$ even though the 'source term' on the right-hand side of (2.34) depends only on the slow variable $x_1$ (which might suggest seeking a solution that is independent of $X$, cf. Lighthill 1954). However, as was pointed out by Smith (1982) and Elliott & Smith (1987), this short lengthscale develops naturally in the solution of the initial-value problem and its exclusion from (2.46) and (2.47) would preclude any possibility of instability waves appearing in the flow.

Our decision to include this term is based on a preliminary analysis of the problem. The details are rather tedious, but the major points can be outlined as follows. The straightforward Lighthill-type approach turns out to be non-uniformly valid at small values of $\mathscr{S}_0$ and an inner (i.e. low-frequency) expansion has to be worked out in order to render it uniformly valid there. It turns out that the correct inner solution is governed by an inhomogeneous form of the equation considered by Ryzhov & Smith (1984).

Its solution develops a finite time singularity (due to the rapid growth of its small-wavelength components) which can be deferred (see (2.88) and f.f.) by rendering it uniformly valid on the length and frequency scales $X = O(1)$ and $\mathscr{S}_0 = O(1)$ respectively. This can be done by using the method of matched asymptotic expansions. The outer solution in the relevant composite expansion satisfies an inhomogeneous equation of the form (2.46) (with $v_1$ determined by (2.47) and the derivatives with respect to the fast 'variable' $X$ included). But this shows that the Lighthill-type scaling, which led to the original outer solution, must have been incorrect and that the terms involving $X$ should have been retained at the outset.

We note that two scaled streamwise coordinates are not being treated as independent variables (as in the usual method of multiple scales), and that (2.46) and (2.47)

will be solved exactly without making any use of the fact that the $Y^2\partial u_1/\partial X$, $Yv_1$, and $\mathrm{d}p_0/\mathrm{d}X$ terms are formally small in a strict asymptotic sense. A similar approach is described by Stewartson (1981) for an almost inviscid critical layer, where a small viscous term is promoted in order to resolve an exponentially large, violently oscillatory solution.

We shall see that the resulting solution involves instability waves that rapidly grow to dominate over the $X$-independent forced solution in the region where $x_1 = O(1)$, even though their initial amplitude is exponentially small. This in itself can be considered as sufficient reason for retaining the formally small convective terms in (2.46). The only question we do not completely answer is whether our procedure misses some combination of eigensolutions that are of higher algebraic order but have numerically smaller factors in the exponent. But since we solve the equations exactly, that could only occur if there were additional small terms that should have been retained in the equations.

### 2.3. *The solution*

Differentiating (2.46) with respect to $X$, using (2.37) and the definitions (2.4), and (2.24)–(2.26), and finally using (2.47) to eliminate $u_1$ we obtain

$$\mathrm{L}v_1 = -\frac{\mathrm{d}^2 p_0}{\mathrm{d}X^2} - \epsilon^{\frac{1}{3}}\mu A'' Y\left(1 - \tfrac{1}{2}Y\frac{\mathrm{d}}{\mathrm{d}Y}\right)u_0 \tag{2.48}$$

and

$$\frac{\partial v_1}{\partial Y} = v_1 = 0 \quad \text{for } Y = 0, \tag{2.49}$$

where the operator L is defined by

$$\mathrm{L} \equiv \mathrm{i}\mathscr{S}_0\frac{\partial}{\partial Y} - \mu^{\frac{1}{2}}Y^2\frac{\partial^2}{\partial X\,\partial Y} - \mu Y\frac{\partial}{\partial X} + \frac{\partial^3}{\partial Y^3}.$$

These equations must be solved subject to an appropriate matching condition. They possess a solution of the form

$$v_1 = \mu\int_{-\infty}^{\infty} g(Y, X-\tilde{X})\,A''(\tilde{x}_1)\,\mathrm{d}\tilde{x}_1, \tag{2.50}$$

$$p_0 = \mu\int_{-\infty}^{\infty} q(X-\tilde{X})\,A''(\tilde{x}_1)\,\mathrm{d}\tilde{x}_1, \tag{2.51}$$

provided $g$ and $q$ satisfy

$$\mathrm{L}g + \frac{\mathrm{d}^2 q}{\mathrm{d}X^2} = -\delta(X-\tilde{X})\,Y\left(1 - \tfrac{1}{2}Y\frac{\mathrm{d}}{\mathrm{d}Y}\right)u_0 \tag{2.52}$$

and

$$g = \frac{\partial g}{\partial Y} = 0 \quad \text{for } Y = 0. \tag{2.53}$$

Correspondingly, $a$ will have the representation

$$a = \mu\int_{-\infty}^{\infty} h_{\mathscr{S}_0}(X-\tilde{X})\,A''(\tilde{x}_1)\,\mathrm{d}\tilde{x}_1, \tag{2.54}$$

where $h_{\mathscr{S}_0}$ is related to $g$ by the matching condition

$$g \sim -\tfrac{1}{2}\mu\frac{\mathrm{d}h_{\mathscr{S}_0}}{\mathrm{d}X}Y^2 \quad \text{as } Y \to \infty, \tag{2.55}$$

which follows from (2.5), (2.39) and (2.43). Also $q(X-\tilde{X})$ is related to $h_{\mathscr{S}_0}(X-\tilde{X})$ by

$$\frac{\mathrm{d}h_{\mathscr{S}_0}}{\mathrm{d}X} = \frac{1}{\pi}\int_{-\infty}^{\infty} \frac{q(\tilde{X}-\tilde{X})}{\tilde{X}-X}\,\mathrm{d}\tilde{X}, \tag{2.56}$$

which follows from (2.45).

In writing (2.50), (2.51) and (2.54), we have implicitly adopted a modified Green-function approach in which the Green function $h_{\mathscr{S}_0}$ depends only on the fast variable $X$ while the source function depends only on the slow variable $x_1$. We could also have proceeded, perhaps more directly, by treating $X$ and $x_1$ as if they were of the same order and taking Fourier transforms of (2.48) with respect to $X$ (or $x_1$). However, we are actually seeking a causal solution to an initial-value problem, which forces us to consider (in §2.4 below) the limiting form of the solution as $\mathscr{S}_0 \to 0$ in order to discuss its matching with an appropriate inner solution, which is valid when $\mathscr{S}_0 = O(\epsilon^2 R^{-\frac{1}{10}})$. This solution depends only on the slow variable $x_1$ and, as will be shown below, it turns out to be especially convenient to demonstrate that the 'Green function' $h_{\mathscr{S}_0}$ actually depends on this variable and not on $X$ when $\mathscr{S}_0 = O(\epsilon^2 R^{-\frac{1}{10}})$.

Introducing the 'fast-variable' Fourier transform

$$\bar{g} = \int_{-\infty}^{\infty} \mathrm{e}^{-\mathrm{i}k(X-\tilde{X})} g\,\mathrm{d}X, \tag{2.57}$$

and similarly for $\bar{h}$ and $\bar{q}$, we find from (2.50) and (2.52) that

$$\bar{g}_0 \equiv \bar{g} + \frac{u_0}{\mathrm{i}\mu k}$$

satisfies

$$\bar{g}_0''' + \mathrm{i}(\mathscr{S}_0 - \tfrac{1}{2}\mu k Y^2)\bar{g}_0' + \mathrm{i}k\mu Y \bar{g}_0 = k^2\bar{q}, \tag{2.58}$$

$$\bar{g}_0' = \frac{-(\mathrm{i}\mathscr{S}_0)^{\frac{1}{2}}}{\mu k}; \quad \bar{g}_0 = 0 \quad \text{for } Y = 0, \tag{2.59}$$

$$\bar{g}_0 \sim -\tfrac{1}{2}\mathrm{i}\mu k Y^2 \bar{h}_{\mathscr{S}_0} \quad \text{as } Y \to \infty, \tag{2.60}$$

$$\bar{h}_{\mathscr{S}_0} = \frac{|k|}{k^2}\bar{q}, \tag{2.61}$$

where the prime now denotes differentiation with respect to $Y$, and we define the analytic function

$$|k| \equiv [(k+\mathrm{i}0)(k-\mathrm{i}0)]^{\frac{1}{2}} \tag{2.62}$$

with the branch of the square roots chosen to make $\mathrm{Re}\,|k| \geqslant 0$. Putting

$$s \equiv \frac{\mathrm{i}\mathscr{S}_0}{(2\mathrm{i}k\mu)^{\frac{1}{2}}}, \tag{2.63}$$

and introducing the new variables (see Lyne 1970)

$$\eta \equiv \tfrac{1}{2}(2\mathrm{i}k\mu)^{\frac{1}{2}} Y^2 \tag{2.64}$$

and

$$Z \equiv \tfrac{1}{2}\mathrm{i}k\mu \frac{\mathrm{d}^2\bar{g}_0}{\mathrm{d}\eta^2} \tag{2.65}$$

into (2.58), we obtain, upon dividing by $\eta^{\frac{1}{2}}$ and differentiating the result with respect to $\eta$,

$$\eta Z'' + \tfrac{5}{2}Z' + \tfrac{1}{2}(s - \tfrac{1}{2}\eta)Z = -\frac{k^2\bar{q}(2\mathrm{i}k\mu)^{\frac{1}{2}}}{16\sqrt{2}\eta^{\frac{1}{2}}}, \tag{2.66}$$

where the primes now denote differentiation with respect to $\eta$, and the branch cuts for $k^{\frac{1}{2}}$ are taken along the positive imaginary axis so that $(ik)^{\frac{1}{2}} = e^{\pm i\pi/4}|k|^{\frac{1}{2}}$ for $k \gtrless 0$ when $k$ is real. Inserting (2.63)–(2.65) into (2.58) and applying the first boundary condition (2.59), we obtain

$$\frac{d}{d\eta}(\eta^{\frac{3}{2}}Z) = \frac{1}{4\sqrt{2}}[\tfrac{1}{2}k^2\bar{q}(2ik\mu)^{\frac{1}{4}} + is^{\frac{3}{2}}] \quad \text{for } \eta = 0. \tag{2.67}$$

Expressing the second boundary condition (2.59) in terms of $Z$ is somewhat more complicated. To this end we differentiate (2.58) with respect to $Y$, insert (2.63)–(2.65), use (2.66) to eliminate $Z''$, and finally impose the second boundary condition (2.59) to eliminate $\bar{g}_0$. The result is

$$\frac{1}{\eta^{\frac{1}{2}}}\left[\frac{d}{d\eta}(\eta^{\frac{3}{2}}Z) - \frac{k^2\bar{q}(2ik\mu)^{\frac{1}{4}}}{8\sqrt{2}}\right] \sim -\tfrac{1}{4}ik\mu s\frac{d\bar{g}_0}{d\eta} \quad \text{as } \eta \to 0. \tag{2.68}$$

Then integrating (2.65) with respect to $\eta$, using (2.60) and (2.64) and inserting the result into (2.68), finally yields

$$\frac{1}{\eta^{\frac{1}{2}}}\left[\frac{d}{d\eta}(\eta^{\frac{3}{2}}Z) - \frac{k^2\bar{q}(2ik\mu)^{\frac{1}{4}}}{8\sqrt{2}}\right] \sim \tfrac{1}{2}s\left[\int_\eta^\infty Z\,d\eta + \tfrac{1}{8}(2ik\mu)^{\frac{3}{2}}\bar{h}_{\mathscr{S}_0}\right] \quad \text{as } \eta \to 0. \tag{2.69}$$

Both sides of this equation become infinite as $\eta \to 0$ but, as we shall see, the singular parts cancel out and the remaining finite terms provide a proper boundary condition for $Z$.

Equation (2.66) is easily transformed into an inhomogeneous Kummer's equation, and its solutions can therefore be expressed in terms of confluent hypergeometric functions. The solution that remains bounded at infinity can be written as

$$Z = \frac{(2ik\mu)^{\frac{1}{4}}k^2\bar{q}}{16\sqrt{2}}[W(M_{\frac{3}{4}}, U_{\frac{3}{4}}) + c_2\,U_{\frac{3}{4}}], \tag{2.70}$$

where $c_2$ is a constant, the primes still denote differentiation with respect to $\eta$,

$$W(s,\eta) \equiv W(M_{\frac{3}{4}}, U_{\frac{3}{4}}) = M_{\frac{3}{4}}U'_{\frac{3}{4}} - U_{\frac{3}{4}}M'_{\frac{3}{4}} \tag{2.71}$$

denotes the Wronskian of $M_{\frac{3}{4}}$ and $U_{\frac{3}{4}}$ in the usual notation, and we have put

$$U_r(s,\eta) \equiv -\int_\eta^\infty U(\tfrac{5}{4} - \tfrac{1}{2}s, 1+2r, \tilde{\eta})\,e^{-\tilde{\eta}/2}\,d\tilde{\eta}, \tag{2.72}$$

and

$$M_r(s,\eta) \equiv \frac{\Gamma(2\mu - \frac{1}{4} - \frac{1}{2}s)}{\Gamma(2\mu+1)}\int_0^\eta M(\tfrac{5}{4} - \tfrac{1}{2}s, 1+2r, \tilde{\eta})\,e^{-\tilde{\eta}/2}\,d\tilde{\eta}, \tag{2.73}$$

where $U$ and $M$ denote the Kummer confluent hypergeometric functions in the usual notation, i.e. $M$ denotes ${}_1F_1$, and $U \to 0$ as $\mathrm{Re}\,\eta \to \infty$ (see Abramowitz & Stegun 1964, p. 504).

Inserting (2.70) into the boundary condition (2.67) and using the properties of $U$ and $M$ given in Abramowitz & Stegun (1964, p. 504) we find that

$$c_2(2i\mu k)^{\frac{1}{4}}k^2\bar{q} = \frac{i8s^{\frac{1}{2}}\Gamma(\frac{5}{4} - \frac{1}{2}s)}{\pi^{\frac{1}{2}}}. \tag{2.74}$$

Similarly, inserting (2.70) into the boundary condition (2.69), noting that the $O(\eta^{-\frac{1}{2}})$ singular terms cancel out, we obtain

$$-k\bar{q}\left\{\left[sc_2-\frac{4}{\pi^{\frac{1}{2}}}\Gamma(\tfrac{5}{4}-\tfrac{1}{2}s)\right]\frac{\left[U_{\frac{1}{4}}(s+2,0)+\dfrac{2\pi^{\frac{1}{2}}(s+\frac{1}{2})}{\Gamma(\frac{3}{4}-\frac{1}{2}s)}\right]}{(\frac{1}{2}-s)}+\frac{2c_2\pi^{\frac{1}{2}}(\frac{1}{2}+s)}{\Gamma(\frac{3}{4}-\frac{1}{2}s)}+s\int_0^\infty W\,\mathrm{d}\eta\right\}=(\sqrt{2})4\mathrm{i}\mu s(2\mathrm{i}k\mu)^{\frac{1}{4}}\bar{h}_{\mathscr{S}_0}. \quad (2.75)$$

Finally, using (2.61) and (2.74) to eliminate $c_2$ and $\bar{q}$, yields

$$\bar{h}_{\mathscr{S}_0}=\frac{4\mathrm{i}s^{\frac{3}{2}}}{(2\mathrm{i}k\mu)^{\frac{3}{4}}\Delta}\left[U_{\frac{1}{4}}(s+2,0)+\frac{\pi(\frac{1}{2}+s)}{s\Gamma(\frac{3}{4}-\frac{1}{2}s)}\right], \quad (2.76)$$

where we have put

$$\Delta\equiv\Delta(k)\equiv-\frac{s\pi^{\frac{1}{2}}}{\Gamma(\frac{1}{4}-\frac{1}{2}s)}\left[\beta\int_0^\infty W\,\mathrm{d}\eta+2^{\frac{3}{2}}\right]+2\beta\left[U_{\frac{1}{4}}(s+2,0)+\frac{2\pi^{\frac{1}{2}}(\frac{1}{2}+s)}{\Gamma(\frac{3}{4}-\frac{1}{2}s)}\right] \quad (2.77)$$

and

$$\beta\equiv\frac{k^3}{2\mathrm{i}\mu|k|(2\mathrm{i}k\mu)^{\frac{1}{4}}}. \quad (2.78)$$

Since (2.54) is of convolution form, (2.4), (2.24), (2.26), (2.38) and the definition (2.57) of the Fourier transform show that the streamwise velocity fluctuation amplitude in the main boundary layer is given by

$$\tilde{u}_{\mathscr{S}}=\epsilon^2U_0'\frac{\lambda_0'}{2\pi}\int_{-\infty}^{\infty}\mathrm{e}^{\mathrm{i}kX}\bar{h}_{\mathscr{S}_0}(k)\,A^{\mathrm{T}}\left(\frac{k}{\epsilon^{\frac{4}{5}}}\right)\mathrm{d}k, \quad (2.79)$$

where

$$A^{\mathrm{T}}(k)\equiv\frac{\mu}{\lambda_0'}\int_{-\infty}^{\infty}\mathrm{e}^{-\mathrm{i}k\tilde{x}_1}A''(\tilde{x}_1)\,\mathrm{d}\tilde{x}_1 \quad (2.80)$$

is the Fourier transform of $\mu A''/\lambda_0'$ in terms of the 'slow' streamwise variable $\tilde{x}_1$.

### 2.4. *The eigensolution and the steady-state causal solution*

The equation

$$\Delta(\kappa_n)=0 \quad (2.81)$$

possesses an infinite set of simple roots, say $\kappa_n$ for $n=2,3,4,\ldots$, which have positive real and imaginary parts when the Strouhal number $\mathscr{S}$ is real (see Elliott & Smith 1987, for a related result). It also possesses a root, say $\kappa_1$, that lies in the lower half-plane when the Strouhal number $\mathscr{S}$ is real but moves into the upper half-plane when $\mathscr{S}$ has a positive imaginary part.

To obtain the steady-state causal solution the integration contour in (2.31)–(2.33) must be deformed onto the real axis without crossing a singularity of (2.79) (as explained beneath (2.37)). This, in turn, requires that we simultaneously deform the integration contour in (2.79) so that it always lies below the pole at $\kappa_1$ in its integrand as $C\to0$. The path of $\kappa_1$ was traced numerically as $\mathrm{Im}\,\mathscr{S}_0\to0$ for various (fixed) $\mathrm{Re}\,\mathscr{S}_0$, and the results are represented by the solid curves of figure 3. Also shown in this figure are the $\mathscr{S}_0\to0$ asymptote of Elliott & Smith (1987) (short-dashed curve) and the $\mathscr{S}_0\to\infty$ limit

$$\frac{2\kappa_1}{\mu^{\frac{5}{7}}}\sim\left(\frac{2}{\pi}\right)^{\frac{2}{5}}\left(\frac{4\mathscr{S}_0}{\mu^{\frac{8}{7}}}\right)^{\frac{3}{5}}\exp\left(\frac{-\mathrm{i}\pi}{5}\right)-\frac{4}{5}\left(\frac{2}{\pi}\right)^{\frac{8}{5}}\left(\frac{4\mathscr{S}_0}{\mu^{\frac{8}{7}}}\right)^{-\frac{1}{10}}\exp\left(\frac{-11\mathrm{i}\pi}{20}\right) \quad (2.82)$$

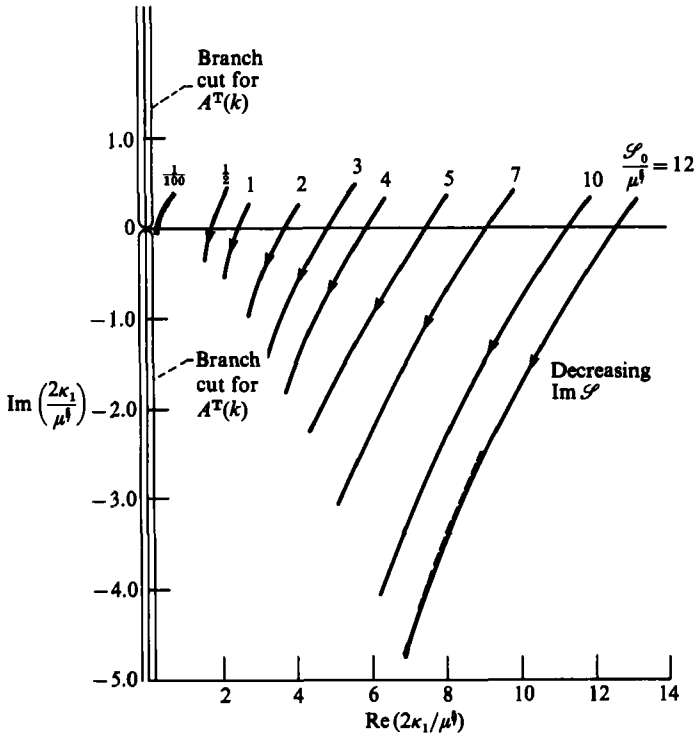


FIGURE 3. Path of roots of dispersion relation (2.81) as Im $\mathscr{S} \to 0$: ---, equation (2.82); -----, low-frequency asymptote from Elliott & Smith (1987).

(long-dashed curve), where the leading term in (2.82) is that obtained by Elliott & Smith (1987). Figure 3 shows that as Im $\mathscr{S}_0 \to 0$, $\kappa_1$ always moves into the lower half-plane without ever intersecting another root of (2.81). This ensures that the factor $\bar{h}_{\mathscr{S}_0}$ will not preclude the required deformation of the integration contour in (2.79). When this deformation is carried out $A^T$ must be analytically continued into the complex $k$-plane. The result cannot be analytic everywhere in this plane because the integral in (2.80) exists only for real $k$. $A^T$ turns out to have branch cuts along the entire imaginary axis for the $A''$ of interest here (see (2.91) below). The integration contour of (2.79) must therefore pass through $k = 0$, but this does not conflict with the deformation imposed by the $h_{\mathscr{S}_0}$ factor because $\kappa_1$ never crosses $k = 0$ as Im $\mathscr{S}_0 \to 0$.

Having deformed the integration contours in (2.31)–(2.33) onto the real-$\mathscr{S}$ axis, we must now consider the behaviour of the integrand at $\mathscr{S}_0 = 0$. Equations (2.76)–(2.78) show that

$$\bar{h}_{\mathscr{S}_0} \sim \frac{2\pi}{\mu k\left[\frac{\pi^{\frac{1}{2}}}{2^4\mu^3}(2i\mu k)^{\frac{3}{2}} + \mathscr{S}_0\right]}, \tag{2.83}$$

and

$$h_{\mathscr{S}_0} \sim \int_{-\infty}^{\infty} \frac{e^{ik(X-\bar{X})}\,dk}{\left[\frac{\pi^{\frac{1}{2}}}{2^4\mu^3}(2i\mu k)^{\frac{3}{2}} + \mathscr{S}_0\right]\mu k} \tag{2.84}$$

as $\mathscr{S}_0 \to 0$. These suggest that $k$ and $X - \bar{X}$ should scale as $\mathscr{S}_0^{\frac{1}{3}}$ and $\mathscr{S}_0^{-\frac{1}{3}}$ respectively as $\mathscr{S}_0 \to 0$, and (2.79) shows that $\tilde{u}_{\mathscr{S}}$ has an integrable branch-point singularity of

$O(\mathscr{S}_0^{-\frac{7}{9}})$ at $\mathscr{S}_0 = 0$ (see (2.91) below). It is worth noting that the Lighthill-type solution would have a non-integrable singularity there. Strictly speaking, the problem should be rescaled in the manner of Ruban (1982*b*) and Smith (1982) when $\mathscr{S}_0 = O(\epsilon^2 R^{-\frac{1}{10}})$, in which case (2.84) shows that $h_{\mathscr{S}_0}$ depends on the slow scale $x_1 - \tilde{x}_1$, as asserted above. We do not tackle the $\mathscr{S}_0 = O(\epsilon^2 R^{-\frac{1}{10}})$ problem here and assume that any singularity that might exist at $\mathscr{S}_0 = 0$ will be no worse than $O(\mathscr{S}_0^{-\frac{7}{9}}.)$ Then on setting $C = 0$ in (2.31), we find that the contribution from this singularity decays at least like $t^{-\frac{2}{9}}$ as $t \to \infty$ (Carrier, Krook & Pearson 1966, pp. 255–256).

The only other singularity in the integrand of (2.31) (with $C = 0$) is a pole at $\mathscr{S}_0 = S_0$. Then as explained above, the steady-state causal solution exists and is given by $\tilde{u}_S \mathrm{e}^{-\mathrm{i}St}$. The poles of the integrand of this latter quantity, given by (2.79) with $S = \mathscr{S}$, and corresponding to the roots $\kappa_n$ of (2.81), contribute the following terms, say $u_n$, to the result:

$$u_n = \frac{\epsilon^2 \lambda_0'}{\mu S_0} \Lambda A^{\mathrm{T}}\left(\frac{\kappa_n}{\epsilon^{\frac{4}{3}}}\right) U_0' \mathrm{e}^{\mathrm{i}(\kappa_n X - St)}; \quad n = 1, 2, 3, \ldots, \tag{2.85}$$

where

$$s_n \equiv \frac{\mathrm{i}S_0}{(2\mathrm{i}\mu\kappa_n)^{\frac{1}{2}}}, \tag{2.86}$$

$$\Lambda\left(\frac{\mu}{S_0^{\frac{4}{3}}}\right) \equiv -\frac{4 s_n^{\frac{3}{2}}}{\mathrm{d}\Delta/\mathrm{d}s_n}\left[U_{\frac{1}{4}}(s_n + 2, 0) + \frac{\pi^{\frac{1}{2}}(\frac{1}{2} + s_n)}{s_n \Gamma(\frac{3}{4} - \frac{1}{2}s_n)}\right], \tag{2.87}$$

and $A^{\mathrm{T}}(\kappa_n/\epsilon^{\frac{4}{3}})$ denotes the analytic continuation of the Fourier transform (2.80) into the complex $k$-plane.

These are eigensolutions, or better, normal modes, of the original boundary-value problem, but their coefficients, which we refer to as the 'coupling coefficients', are now uniquely determined. The lowest-order mode, which corresponds to $\kappa_1$ and, for reasons given below, is of principal interest here, will exhibit spatial growth in the downstream direction and therefore represents a spatially growing instability wave.

An important consequence of (2.85) can be deduced by considering its limit as $\mathrm{Re}\,(\mathscr{S}_0) \to \infty$. Equation (2.82), and the asymptotic results of Elliott & Smith (1987) show that $-\mathrm{Im}\,(\kappa_1)$ increases like $\mathscr{S}^{\frac{3}{5}}$ as $\mathrm{Re}\,(\mathscr{S}) \to \infty$. The contour integrals (2.31)–(2.33) (on which our analysis is based) cannot, therefore, exist because the contribution of the corresponding pole causes the integrands to grow too rapidly as $\mathrm{Re}\,(\mathscr{S}) \to \infty$. This is due to the non-uniform validity of the present solution at large $\mathscr{S}$. The increase in $-\mathrm{Im}\,(\kappa_1)$ with $\mathscr{S}$ would eventually be reversed at wavelengths comparable with the thickness of the steady boundary layer in the uniformly valid result (that there must be a maximum growth rate follows from the fact that small-wavelength disturbances satisfy the Orr–Sommerfeld equation, whose solutions do not exhibit spatial growth at infinite Strouhal number for sufficiently smooth mean-flow profiles).

A uniformly valid composite solution must be constructed in order to obtain convergence. Its Fourier transform, with respect to $X$, can be written as

$$\bar{v}_{1,\mathrm{T}}(k, \mathscr{S}) + \bar{v}_{1,\mathrm{R}}(k, \mathscr{S}) - \bar{v}_{1,\mathrm{TR}}(k, \mathscr{S}), \tag{2.88}$$

where $\bar{v}_{1,\mathrm{T}}(k, \mathscr{S})$ is the Fourier transform of the present solution to the boundary-value problem (2.48) and (2.49), $\bar{v}_{1,\mathrm{R}}(k, \mathscr{S})$ is the solution to this problem with the linear operator L replaced by the appropriate Rayleigh scale operator, and $\bar{v}_{1,\mathrm{TR}}$ denotes the simplified solution in the wavenumber space overlap domain for these two solutions.

The Briggs (1964)–Bers (1975) procedure can now be applied, as above, to the

composite expansion (2.88) to determine the net contribution of the instability wave to the unsteady solution. The former is determined by a pole that occurs at relatively low wavenumbers for the relatively small source Strouhal number (2.26). In which case, the contribution from the corresponding instability-wave pole in $\bar{v}_{1,\mathrm{R}}$ will be cancelled by the one in $\bar{v}_{1,\mathrm{TR}}$, since the latter must have nearly the same residue at these low wavenumbers. The instability wave is, therefore, still given by (2.85) with $n = 1$, which shows that the solution only has to be uniformly valid over timescales that are long enough to resolve the instability wave of interest.

The $\bar{v}_{1,\mathrm{R}}$ pole would contribute only at a much larger value of $S$. But it is still necessary to continuously deform the integration contour around this pole in the limit as $\mathrm{Im}\,\mathscr{S} \to 0^+$. This is possible only when the flow exhibits convective and not absolute instability. The latter usually occurs when the mean motion involves some reversed flow.

Moore (1979) showed that similar behaviour occurs in analyses, such as the one of Crighton & Leppington (1974), of the small-amplitude unsteady motion on velocity discontinuity shear layers – presumably because the discontinuous profile is inappropriate for sufficiently small-wavelength disturbances.

### 2.5. *Non-interactive steady marginal separation*

We now concentrate on flows that are relatively far from separation (since this is probably the case of most experimental interest); the scaled minimum wall shear

$$\tau_0 \equiv \tau_{\min} R^{\frac{1}{8}}, \tag{2.89}$$

should then be somewhat greater than unity. In such a case $\mu A$ should not be very different from its limiting (i.e. non-interactive) form, as pointed out by Stewartson *et al.* (1982), i.e.

$$\mu A \sim [(x_1 \lambda_0')^2 + \tau_0^2]^{\frac{1}{2}}. \tag{2.90}$$

In which case (2.80) becomes

$$A^{\mathrm{T}}(k) \sim 2\left(\frac{\tau_0 |k|}{\lambda_0'}\right) K_1\left(\frac{\tau_0 |k|}{\lambda_0'}\right), \tag{2.91}$$

where $K_1$ is the modified Bessel function of the second kind in the usual notation and $|k|$ is defined by (2.62). It therefore follows from the asymptotic expansion of $K_1$ (Abramowitz & Stegun 1964, p. 378) that

$$A^{\mathrm{T}}\left(\frac{\kappa_n}{\epsilon^{\frac{6}{5}}}\right) \sim \left(\frac{2\pi\tau_0 \kappa_n}{\lambda_0' \epsilon^{\frac{6}{5}}}\right)^{\frac{1}{2}} \left[\exp\left(-\frac{\tau_0 \kappa_n}{\lambda_0' \epsilon^{\frac{6}{5}}}\right)\right] [1 + O(\epsilon^{\frac{6}{5}})], \tag{2.92}$$

which is exponentially small, since $\mathrm{Re}\,\kappa_n > 0$ for $n = 1, 2, 3$ etc. This suggests that the coupling coefficient should be $O(\epsilon^{\frac{7}{5}} \exp\{-[\tau_0/(\lambda_0' \epsilon^{\frac{6}{5}})]\,\mathrm{Re}\,\kappa_n\})$ – an estimate that we expect to remain valid even when $\tau_0$ is not large.

While the coupling coefficient is exponentially small in a formal asymptotic sense, in reality it cannot be very far from unity, since $\epsilon^{-\frac{6}{5}} = R^{\frac{3}{35}}$ cannot be very large for any laminar flow. It is worth noting that the complete term (2.85) is exponentially large when $\epsilon^{\frac{6}{5}} X \gg 1$ and $n = 1$ even though the coupling coefficient is exponentially small. The contribution (2.85) then dominates the remaining terms in the solution, which have only algebraic order. It must therefore be included in order to render the solution uniformly valid in $X$, which must be accomplished before considering its development in the larger outer region. Finally it is worth noting that there is precedent in the literature for including exponentially small terms along with

algebraically small terms (see Van Dyke 1975, p. 256, note 11; Dingle 1973, pp. 5–19) even if our composite expansion procedure cannot be completely justified in the formal Poincaré sense.

## 3. The outer solution

Our primary interest is in the subsequent evolution of the normal modes (2.85) as they emerge downstream from the region of marginal separation.

### 3.1. *The mean flow*

It follows from (2.5), (2.6), (2.9) and (2.22) that

$$U \sim \lambda_0' R^{-\frac{1}{8}} x_1 y + \tfrac{1}{2}\mu y^2 \quad \text{as } x_1 \to +\infty \quad \text{with } y \ll 1. \tag{3.1}$$

But the static pressure decreases from its maximum near the point $x_c$ like $x^{-\frac{1}{2}}$ for thin bodies at high angles of attack and eventually becomes of the order of the small angle of attack $\sigma$ for $x \gg 1$. The variation of the scaled wall shear $\tau$ is then controlled by the viscous-boundary-layer growth. Thus $\tau$ first increases rapidly (on the scale of $x$) to an $O(1)$ value, say $x^{\frac{1}{2}}T(x, R)$, and ultimately remains constant on an even longer scale as $x \to \infty$.

The mean velocity profile therefore behaves like

$$\left.\begin{aligned} U &= \epsilon^2[\lambda(x; R)\, Y + \tfrac{1}{2}\mu Y^2 + \ldots] && (3.2)\\ V &= -\epsilon^{10}\tfrac{1}{2}\frac{\mathrm{d}\lambda}{\mathrm{d}x} Y^2 && (3.3) \end{aligned}\right\} \quad \text{for } Y = O(1), \quad x_1 \gg 1,$$

where

$$\lambda(x, R) \equiv \frac{T(x, R)}{\epsilon} \tag{3.4}$$

and

$$T \sim \begin{cases} \lambda_0'(x - x_c) & \text{as } x \to x_c \\ \dfrac{\lambda_B}{\sqrt{2}}\left(\dfrac{U_\infty}{U_e}\right)^{\frac{3}{2}}\left(\dfrac{1}{x^{\frac{1}{2}}} - \dfrac{b_0}{x} + \dfrac{b_1}{x^{\frac{3}{2}}}\ln x^{\frac{1}{2}} + \dfrac{b_2}{x^{\frac{3}{2}}}\right) + O(x^{-2}\ln x) & \text{as } x \to \infty, \end{cases} \tag{3.5}$$

where $\lambda_B = 0.4696\ldots$ is the scaled Blasius wall shear and the $b$ are $O(1)$ constants, which are easily deduced by using thin-airfoil theory in conjunction with the linearized boundary-layer equation. From (3.2) and (3.5) we see that the mean flow shear term is no longer much smaller than the pressure-gradient term in the lower layer when

$$x - x_c = O(\epsilon). \tag{3.6}$$

We therefore introduce an intermediate region in which

$$x_2 \equiv \frac{x - x_c}{\epsilon} \tag{3.7}$$

is order one. The latter is much larger (in a formal asymptotic sense) than the original marginally separated region $x - x_c = O(R^{-\frac{1}{8}})$. Notice that $\lambda = O(\epsilon^{-1})$ in the even larger outer region where $x - x_c = O(1)$ (see figure 2).

### 3.2. *The unsteady solution*

The solutions (2.85), which are valid in the region of marginally separated flow, do not remain valid in either of the two outer regions referred to at the end of §3.1, but we expect that they will evolve into the correct solutions in a gradual fashion. The latter can be obtained by the method of multiple scales (Nayfeh 1973) as was done by Goldstein (1983) for the asymptotic eigensolutions of the unsteady boundary-layer equation.

We therefore seek a solution for the normal mode of the form

$$\tilde{u} \sim U' a_0(x_2) \exp\left[\frac{\mathrm{i}}{\epsilon^3}\int_0^{x_2} \kappa(x_2')\,\mathrm{d}x_2'\right], \tag{3.8}$$

where $U$ still denotes the streamwise component of the mean flow velocity (which now depends on the slow streamwise coordinate only through the slow variable $x_2$); the prime on $U$ denotes differentiation with respect to $y$; $a_0$ and $\kappa$ depend on $R$ (and ultimately on the slower variable $x_2$) and $a_0$ is of the order of magnitude of the coupling coefficient alluded to at the end of §2. (Note that the eigenmode dominates the free-stream disturbance in this region.)

This then provides a first approximation to the solution of the linearized momentum and continuity equations in the region $x_2, y = O(1)$ provided (see (2.39))

$$\tilde{v} \sim -\mathrm{i}U\kappa a_0(x_2) \exp\left[\frac{\mathrm{i}}{\epsilon^3}\int_0^{x_2} \kappa(x_2')\,\mathrm{d}x_2'\right], \tag{3.9}$$

and

$$\tilde{p} \sim \epsilon^3 \hat{p}_0(x_2)\, a_0(x_2) \exp\left[\frac{\mathrm{i}}{\epsilon^3}\int_0^{x_2} \kappa(x_2')\,\mathrm{d}x_2'\right], \tag{3.10}$$

where the slow streamwise dependence of $\hat{p}_0$ on $x_2$ is also explicitly indicated.

This will match onto a potential flow in the outer region where $y/R^{\frac{3}{10}} = O(1)$, and the requirement that the latter decay exponentially as $y/R^{\frac{3}{10}} \to \infty$ can only be met if

$$\hat{p}_0 = \kappa. \tag{3.11}$$

The solution in the viscous wall layer, where $Y = O(1)$, must then be of the form

$$\tilde{u} \sim \epsilon G'(Y, x_2) \exp\left[\frac{\mathrm{i}}{\epsilon^3}\int_0^{x_2} \kappa(x_2')\,\mathrm{d}x_2'\right], \tag{3.12}$$

$$\tilde{v} \sim -\epsilon^2 \mathrm{i} G(Y, x_2)\, \kappa(x_2) \exp\left[\frac{\mathrm{i}}{\epsilon^3}\int_0^{x_2} \kappa(x_2')\,\mathrm{d}x_2'\right], \tag{3.13}$$

$$\tilde{p} \sim \epsilon^3 \kappa a_0 \exp\left[\frac{\mathrm{i}}{\epsilon^3}\int_0^{x_2} \kappa(x_2')\,\mathrm{d}x_2'\right], \tag{3.14}$$

where the prime now denotes differentiation with respect to $Y$ and $G$ satisfies the equation

$$G''' + \mathrm{i}[S_0 - \kappa(\lambda Y + \tfrac{1}{2}\mu Y^2)]\, G' + \mathrm{i}\kappa(\lambda + \mu Y)\, G = \mathrm{i}\kappa^2 a_0, \tag{3.15}$$

subject to the homogeneous boundary conditions

$$G = G' = 0 \quad \text{at } Y = 0. \tag{3.16}$$

Introducing the new variables

$$\zeta = \tfrac{1}{2}(2\mathrm{i}\kappa\mu)^{\frac{1}{2}}\left(Y+\frac{\lambda}{\mu}\right)^2, \tag{3.17}$$

$$H \equiv \tfrac{1}{2}\mathrm{i}\kappa\mu\frac{\mathrm{d}^2G}{\mathrm{d}\zeta^2}, \tag{3.18}$$

and

$$\tilde{s} \equiv \frac{\mathrm{i}}{(2\mathrm{i}\kappa\mu)^{\frac{1}{2}}}\left(S_0+\frac{\lambda^2\kappa}{2\mu}\right) = s^* + \tfrac{1}{2}\zeta_0, \tag{3.19}$$

where

$$\zeta_0 = \tfrac{1}{2}(2\mathrm{i}\kappa\mu)^{\frac{1}{2}}\left(\frac{\lambda}{\mu}\right)^2, \tag{3.20}$$

and

$$s^* \equiv \frac{\mathrm{i}S_0}{(2\mathrm{i}\kappa\mu)^{\frac{1}{2}}}, \tag{3.21}$$

we obtain upon differentiation

$$\zeta H'' + \tfrac{5}{2}H' + \tfrac{1}{2}(\tilde{s}-\tfrac{1}{2}\zeta)\,H = -\frac{\kappa^2\mathrm{i}(2\mathrm{i}\kappa\mu)^{\frac{1}{4}}a_0}{16\sqrt{2}\zeta^{\frac{3}{2}}}, \tag{3.22}$$

where the primes now denote differentiation with respect to $\zeta$.

Expressed in terms of these new variables, (3.22) is nearly identical with (2.66). The solution that does not grow exponentially as $Y\to\infty$ is therefore given by

$$H = \frac{(2\mathrm{i}\kappa\mu)^{\frac{1}{4}}\mathrm{i}\kappa^2 a_0}{16\sqrt{2}}\,[\tilde{W}(\tilde{s},\zeta)+c_3\,U_{\frac{3}{4}}'(\tilde{s},\zeta)], \tag{3.23}$$

where

$$\tilde{W} \equiv W - M_{\frac{3}{4}}(\tilde{s},\zeta_0)\,U_{\frac{3}{4}}'(\tilde{s},\zeta), \tag{3.24}$$

and $W$, $U_r$ and $M_r$ are still given by (2.71)–(2.73).

Matching with the main-deck solution (3.9) shows that

$$G \sim \tfrac{1}{2}\mu\left(Y^2+\frac{2\lambda}{\mu}\,Y\right)a_0 \quad \text{as } Y\to\infty. \tag{3.25}$$

Inserting (3.17)–(3.21) into (3.15) and using the boundary conditions (3.16) shows that

$$\zeta\frac{\mathrm{d}H}{\mathrm{d}\zeta}+\tfrac{3}{2}H = \frac{\mathrm{i}\kappa^2(2\mathrm{i}\kappa\mu)^{\frac{1}{4}}a_0}{8(2\zeta_0)^{\frac{1}{2}}} \quad \text{at } \zeta=\zeta_0, \tag{3.26}$$

while (3.18), (3.16) and (3.25) show that

$$\int_{\zeta_0}^{\infty} H\,\mathrm{d}\zeta = -(2\mathrm{i}\kappa\mu)^{\frac{3}{2}}\frac{\mathrm{i}a_0}{8\kappa}. \tag{3.27}$$

Inserting the solution (3.23) and eliminating $c_3$ now leads to the dispersion relation

$$D(\kappa) = 0, \tag{3.28}$$

where

$$D \equiv -\tfrac{1}{2}\zeta_0^{\frac{1}{2}}(\tfrac{1}{2}-\tilde{s})\,[(\tfrac{1}{2}+\tilde{s})\,U_{\frac{1}{4}}'(\tilde{s},\zeta_0)-\zeta_0\,U_{\frac{3}{4}}'(\tilde{s},\zeta_0)]\left[b\int_{\zeta_0}^{\infty}\tilde{W}\,\mathrm{d}\zeta+2^{\frac{3}{2}}\right]$$
$$+\tfrac{1}{2}b(\tfrac{1}{2}-\tilde{s})\,U_{\frac{3}{4}}(\tilde{s},\zeta_0)\{4+\zeta_0^{\frac{1}{2}}U_{\frac{3}{4}}(\tilde{s},\zeta_0)[(\tfrac{1}{2}-\tilde{s})\,M_{\frac{1}{4}}'(\tilde{s},\zeta_0)-\zeta_0\,M_{\frac{3}{4}}'(\tilde{s},\zeta_0)]\}, \tag{3.29}$$

and

$$b \equiv \frac{\kappa^2}{2\mathrm{i}\mu(2\mathrm{i}\kappa\mu)^{\frac{1}{4}}}. \tag{3.30}$$

### 3.3. *Matching with the marginal separation solution*

It follows from (3.6) and (3.19)–(3.21) that $\zeta_0 \to 0$ and $\tilde{s} \to s^*$ as $x_2 \to 0$. Then $\tilde{W} \to W$, and it follows (Abramowitz & Stegun 1964, p. 504), that

$$\zeta_0^{\frac{1}{2}}[(\tfrac{1}{2}+\tilde{s})\,U_{\frac{1}{4}}' - \zeta_0\,U_{\frac{3}{4}}'] \to \frac{\pi^{\frac{1}{2}}\tilde{s}}{\Gamma(\frac{5}{4}-\frac{1}{2}\tilde{s})},$$

and

$$(\tfrac{1}{2}-\tilde{s})\,M_{\frac{1}{4}}' - \zeta_0\,M_{\frac{3}{4}}' \to \frac{4\Gamma(\frac{5}{4}-\frac{1}{2}\tilde{s})}{\pi^{\frac{1}{2}}} \quad \text{as } \zeta_0 \to 0.$$

Hence it follows from (2.77), (2.78), (3.29) and (3.30) that

$$D(\kappa) \to \Delta(\kappa) \quad \text{as } x_2 \to 0$$

and consequently from (3.28) that

$$\kappa \to \kappa_n, \tag{3.31}$$

where $\kappa_n$ is the $n$th root of the marginal separation dispersion relation (2.81).

The streamwise velocity fluctuation (3.12) can then be matched to (2.85) for $n = 1, 2, 3, \ldots$. The matching of the amplitudes determines the initial amplitude and consequently the order of magnitude of the slowly varying amplitude function $a_0$. The appropriate continuation of the solution (2.85) into the downstream region

$$0 < x_2 = O(1)$$

is therefore given by (3.8) in this case.

### 3.4. *Simplified behaviour in region* $x - x_c = O(1)$

The Reynolds-number scaling for the region $x_2 \gg 1$, $x - x_c = O(1)$ is different from that implied by (3.8)–(3.14), which are strictly valid only in the region $x_2 = O(1)$. But since the correct formulas turn out to be simplified versions of (3.8)–(3.16) to lowest approximation, (3.28)–(3.30) remain valid in this region.

Then, since (3.4) and (3.5) show that $\lambda$ is large when $x_2 \gg 1$ and $0 < x - x_c = O(1)$, it follows from (3.19) and (3.20) that $\zeta_0$ and consequently $\tilde{s}$ are large in this region, while scaling arguments such as those of Appendix C suggest that $\kappa$ and $b$ will be small. To obtain an appropriate limiting expression for the dispersion relation (3.28) we first express the confluent hypergeometric function integrals (2.72) and (2.73) in terms of the parabolic cylinder functions† by using the relations

$$U_{\frac{1}{4}}(s,\eta) = -2 \times 2^{\frac{1}{2}(\frac{1}{2}-s)} \int_{(2\eta)^{\frac{1}{2}}}^{\infty} U(1-s,y)\,\mathrm{d}y \tag{3.32}$$

and

$$M_{\frac{1}{4}}(s,\eta) = 2^{\frac{1}{2}(s-\frac{1}{2})} \int_0^{(2\eta)^{\frac{1}{2}}} M(1-s,y)\,\mathrm{d}y, \tag{3.33}$$

$$U_{\frac{3}{4}}(s,\eta) = -\frac{2U_{\frac{1}{4}}'(s+2,\eta) + U_{\frac{1}{4}}(s+2,\eta)}{(\frac{1}{2}-s)}, \tag{3.34}$$

$$M_{\frac{3}{4}}(s,\eta) = -\tfrac{1}{2}(s+\tfrac{3}{2})[M_{\frac{1}{4}}'(s+2,\eta) + \tfrac{1}{2}M_{\frac{1}{4}}(s+2,\eta)] - \frac{2}{\pi^{\frac{1}{2}}}\Gamma(\tfrac{1}{4}-\tfrac{1}{2}s), \tag{3.35}$$

† The reader should note that it is now conventional to use the same symbol for the parabolic cylinder function as for the corresponding confluent hypergeometric function and to distinguish between them by the number of their arguments.

where $U(a, Z) = D_{-a-\frac{1}{2}}(Z)$ denotes the parabolic cylinder function in the usual notation and

$$M(a, Z) \equiv \frac{\Gamma(-\frac{1}{2}+a)}{\Gamma(\frac{3}{2})}[U(a, -Z) - U(a, Z)] \tag{3.36}$$

is a second functionally independent parabolic cylinder function (see Abramowitz & Stegun 1964, (19.12.3), (19.12.4), (13.4.8) and (13.4.21) on pp. 691 and 507). We then use Olver's (1959) large-argument asymptotic expansions for the parabolic cylinder functions and Abramowitz & Stegun (1964, (13.4.18)) on p. 507 to show that

$$\begin{aligned} D &\rightarrow -(2\zeta_0)^{\frac{1}{2}}(\tfrac{1}{2}-\tilde{s})[(\tfrac{1}{2}+\tilde{s})\, U'_{\frac{1}{4}}(\tilde{s}, \zeta_0) - \zeta_0\, U'_{\frac{3}{4}}(\tilde{s}, \zeta_0)] \\ &= -(\tfrac{1}{2}-\tilde{s})\, 2^{\frac{1}{2}(\frac{1}{2}-\tilde{s})}[(\tilde{s}+\tfrac{1}{2})\, U(-\tilde{s}+1, (2\zeta_0)^{\frac{1}{2}}) - U(-\tilde{s}-1, (2\zeta_0)^{\frac{1}{2}})] \\ &= -2^{\frac{1}{2}(\frac{1}{2}-\tilde{s})}[(\tfrac{1}{2}\zeta_0)^{\frac{1}{2}} U(-\tilde{s}, (2\zeta_0)^{\frac{1}{2}}) + 2\tilde{s} U'(-\tilde{s}, (2\zeta_0)^{\frac{1}{2}})] \quad \text{as } \zeta_0 \rightarrow \infty, \end{aligned} \tag{3.37}$$

with $b$ finite and $\tilde{s} = O(\zeta_0)$. This is the dispersion relation for the corresponding *non-interactive* eigensolutions, i.e. the eigensolutions that would have been obtained if the inhomogeneous term in (3.15) were eliminated by setting $\hat{p}_0$ equal to zero in (3.11). It corresponds to letting $\lambda \rightarrow \infty$ with $\lambda S_0^{\frac{1}{2}} = O(1)$ and justifies our comment (in §1) that the unsteady eigensolutions become non-interactive as $x_2 \rightarrow \infty$.

It follows from (3.20) that the last member of (3.37) can be further simplified to

$$D \sim -2[(2^{\frac{1}{2}-\tilde{s}})^{\frac{1}{2}}]\, \tilde{s} U'(-\tilde{s}, (2\zeta_0)^{\frac{1}{2}}) \quad \text{as } x_2 \rightarrow \infty.$$

Hence assuming that $s^* \ll \zeta_0$ (as we shall show to be the case), and putting $\mu_0^2 = 2\tilde{s}$ and

$$t = \left(\frac{\zeta_0}{2\tilde{s}}\right)^{\frac{1}{2}} = 1 - \frac{s^*}{\zeta_0} + \ldots \quad \text{as } \zeta_0 \rightarrow \infty$$

in (B 4) of Appendix B, we find that the dispersion relation (3.27) becomes

$$\mathrm{Ai}'\left(-s^*\left(\frac{2}{\zeta_0}\right)^{\frac{1}{3}}\right) = 0 \quad \text{as } \zeta_0 \rightarrow \infty, \tag{3.38}$$

where Ai′ denotes the Airy-function derivative in the usual notation. This implies that $s^* = O(\zeta_0^{\frac{1}{3}})$, and consequently that $s^* \ll \zeta_0$ as assumed above.

The roots of (3.38), say $\mathrm{e}^{-\mathrm{i}\pi}\rho_n$ for $n = 1, 2, 3, \ldots$, lie along the negative real axis, and it follows from (3.20) and (3.21) that the wavenumber $\kappa$ approaches the wavenumber $\kappa_n^{(0)}$ where

$$\kappa_n^{(0)}([\lambda]) \equiv \frac{1}{\mathrm{i}\lambda}\left(\frac{\mathrm{e}^{\frac{1}{2}\mathrm{i}\pi} S_0}{\rho_n}\right)^{\frac{3}{2}} \quad \text{for } n = 1, 2, 3, \ldots. \tag{3.39}$$

Notice that this result is independent of $\mu$. Changing the quantity in the square bracket will indicate a corresponding change in the right-hand side of this equation.

## 4. Discussion of results

The dispersion relation (3.27) determines $2\mathrm{i}\mu\kappa/S_0^2 = -1/s^{*2}$ as a function of

$$\lambda^* = \frac{\lambda S_0^{\frac{1}{2}}}{\mu} \tag{4.1}$$

and

$$\mu^* = \frac{\mu}{S_0^{\frac{7}{4}}}. \tag{4.2}$$

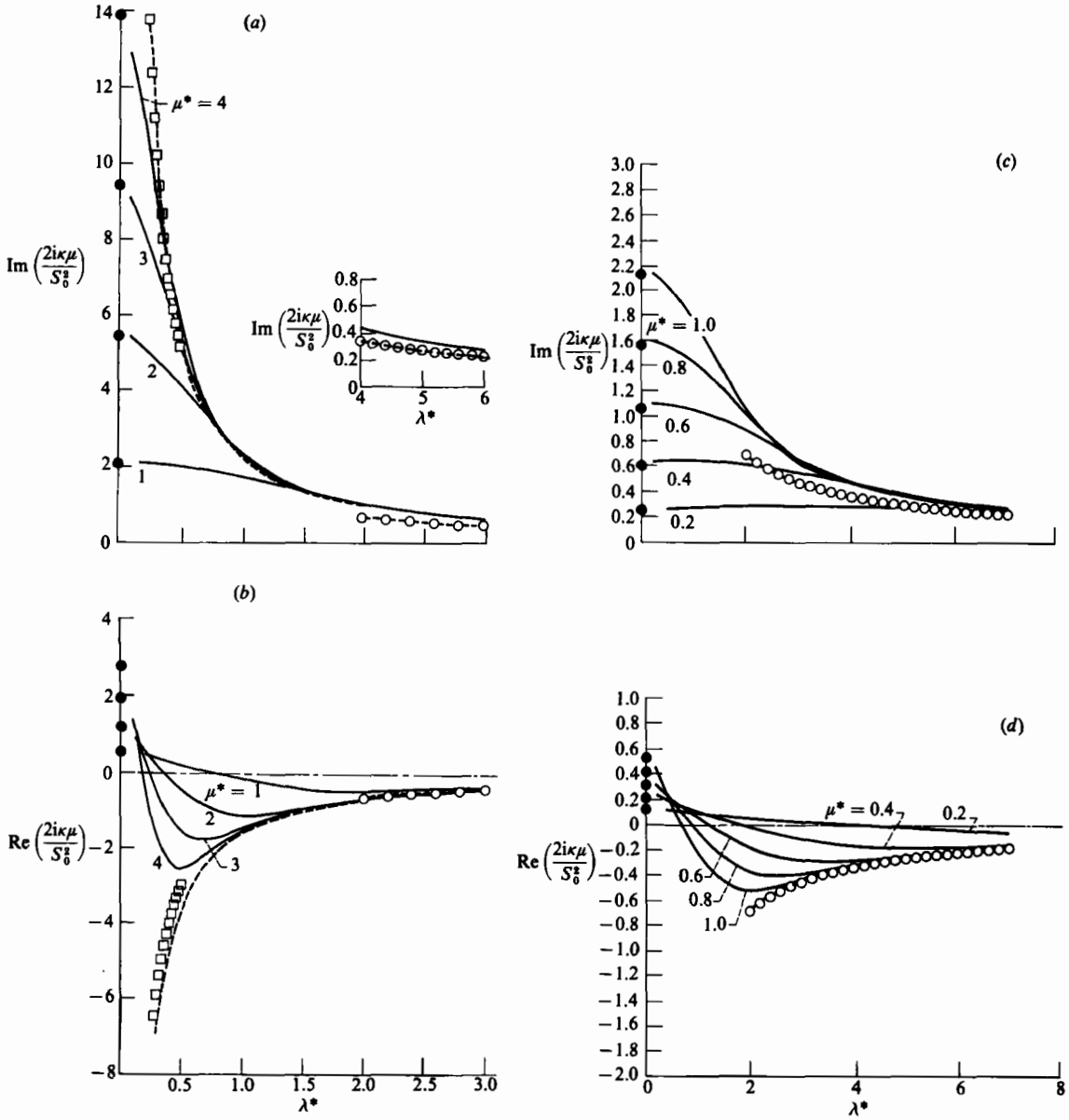


FIGURE 4. Variation of $(a, c)$ the real part, and $(b, d)$ the imaginary part, of the lowest-order $(n = 1)$ root of dispersion relation (3.28) with $\lambda^*$ for various values of $\mu^*$. □, Equation (4.3); ----, root from non-interactive dispersion relation; --○--, equation (3.39); ●, computed from equation (2.81).

The roots $-s^{*-2}$ were computed using Newton iteration to trace out their paths for various values of $\mu^*$ as $\lambda^*$ goes from zero to infinity. Infinite-series representations of the confluent hypergeometric functions were used to compute $U_r$ etc. for small to moderate values of $\lambda^*$, with their large-argument asymptotic expansions also being employed in calculating the integral of the Wronskian. The path of integration was chosen to minimize oscillations of the integrand and obtain fastest convergence. For larger values of $\lambda^*$ the confluent hypergeometric functions were expressed in terms

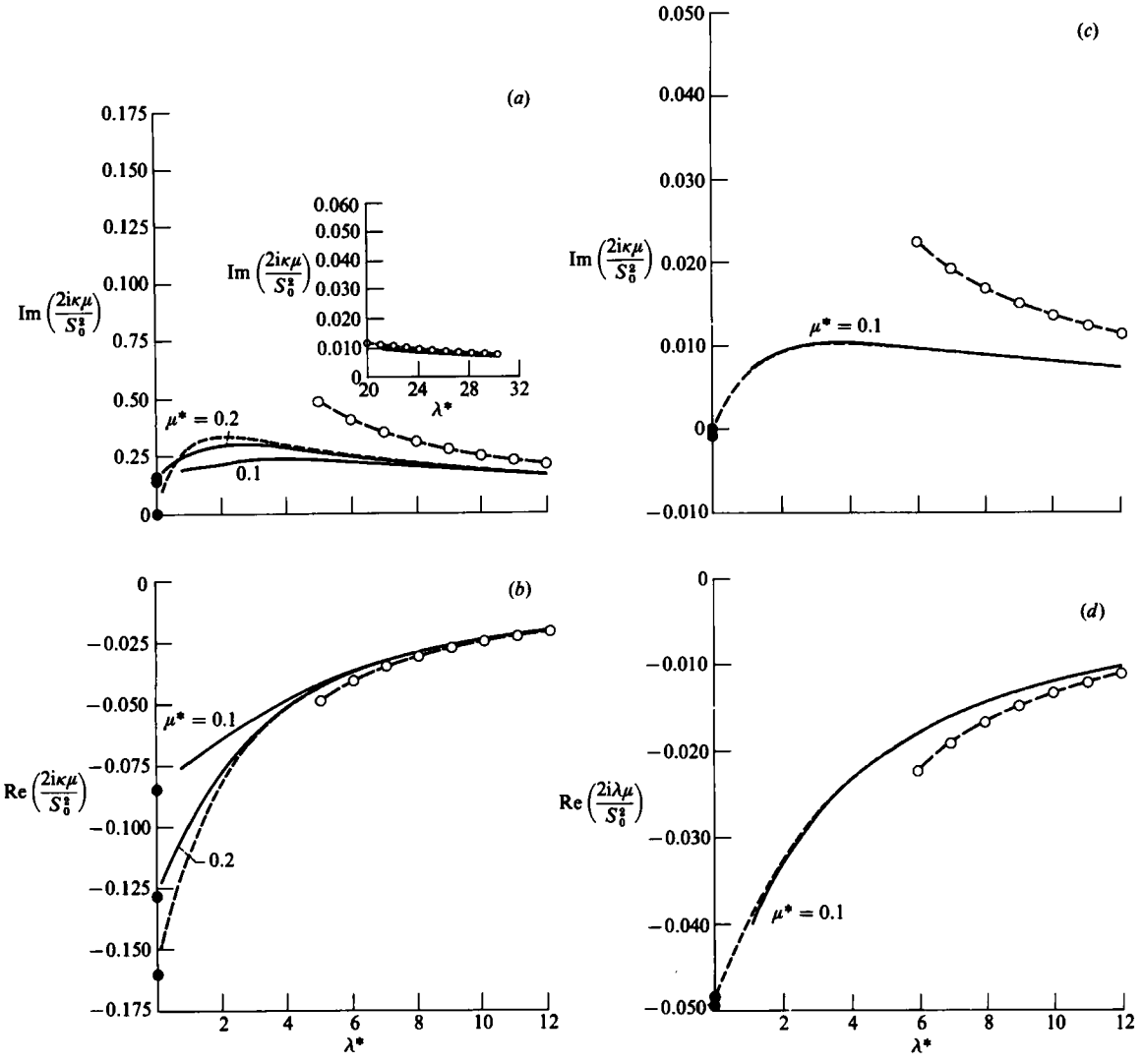


FIGURE 5. Variation of (*a*) the real part, and (*b*) the imaginary part, of second-order ($n = 2$) root of dispersion relation (3.28) with $\lambda^*$ for various values of $\mu^*$. Variation of (*c*) the real part, and (*d*) the imaginary part, of third-order ($n = 3$) root of dispersion relation (3.28) with $\lambda^*$ for various values of $\mu^*$. ----, root from non-interactive dispersion relation; --○--, equation (3.39); ●, computed from equation (2.81).

of parabolic cylinder functions, which were then computed using Olver's (1959) uniformly valid asymptotic expansions. Eigenvalues were also calculated by direct numerical solution of the differential equation and good agreement was found between the results of the different procedures for all cases compared.

The results for the *lowest-order* root are plotted as the solid curves in figure 4. The curve with the open circles is calculated from (3.39). Notice that the wavenumber $\kappa_1^{(0)}$, which corresponds to the lowest-order root $\rho_1$ of (3.38), evolves from the lowest-order root $\kappa_1$ of (2.81). The solid curves approach the dashed curves as $\mu^* \to \infty$ with $\lambda^*$ fixed. The latter are obtained from the non-interactive dispersion relation (3.37) and also approach the curves with the open circles as $\lambda^* \to \infty$. Notice that the lowest-order root of this simplified dispersion relation tends to infinity as $\lambda^* \to 0$.

In fact, expanding (3.37) for small $\lambda^*$, and using the results in Abramowitz & Stegun (1964, p. 687), shows that

$$(2\zeta_0)^{\frac{1}{2}} \sim \frac{8\pi s^*}{\Gamma^2(\frac{1}{4})} \quad \text{as} \quad \frac{\lambda}{\mu} \to 0.$$

Hence it follows from (3.18) and (3.21) that

$$\kappa \sim \kappa_1 \equiv \frac{1}{2\mathrm{i}\mu}\left(\frac{\mu S_0 8\pi\, \mathrm{e}^{\frac{1}{2}\mathrm{i}\pi}}{\lambda \Gamma^2(\frac{1}{4})}\right)^{\frac{4}{3}} \quad \text{as} \quad \frac{\lambda}{\mu} \to 0, \tag{4.3}$$

which is plotted with square symbols on figure 4. Note that (4.3) is not uniformly valid, because the double limits $\mu^* \to \infty$, $\lambda^* \to 0$ do not commute. In fact, the dispersion relation becomes interactive again for $\lambda^* \sim 1/\mu^*$ (see Appendix C and Ruban 1982*b*). This prevents the root from actually becoming infinite, and allows a match with (2.81).

Results for modes $n = 2, 3$ are shown in figure 5. The unbounded wavenumber growth exhibited by the lowest-order non-interactive mode when $\lambda^* \to 0$ suggests that the $n = 1$ mode and $n = 2, 3, 4 \ldots$ modes will have different asymptotic structures in the region of marginally separated flow when $\mu^* \gg 1$ (the $n = 1$ mode is interactive, while the other modes are non-interactive – see Appendix C). Hence *two* asymptotic calculations are necessary to determine all the mode's coupling coefficients for $S_0 \ll 1$. The growing $n = 1$ mode reverts to the Smith–Ryzhov† scaling $S \sim R^{-\frac{1}{20}}$. The appropriate scaling for the other modes, $\tau_{\min} \sim R^{-\frac{1}{5}}$, $S \sim R^{\frac{1}{10}}$ (i.e. $S_0 \sim R^{-\frac{3}{10}}$), leads to larger Tollmien–Schlichting-wave amplitudes and it was for this reason that we initially considered this scaling. However, these modes are of less interest, because they all decay everywhere downstream. We were therefore forced to consider the present scaling in order to find spatially growing instability waves.

The results of Appendix A show that

$$\frac{\mathrm{i}}{\epsilon^3}\int_0^{x_2} \kappa(x_2')\,\mathrm{d}x_2' \sim \frac{S_0^{\frac{3}{2}}}{\epsilon^3 \lambda_0'}\left[\Theta_n(\mu^*) - \left(\frac{\mathrm{e}^{\frac{1}{2}\mathrm{i}\pi}}{\rho_n}\right)^{\frac{3}{2}} \ln\left(\frac{\lambda_0' S_0^{\frac{1}{2}}}{\epsilon\mu}\right)\right] + \frac{\mathrm{i}}{\epsilon^3}\int_{x_c}^{x} \kappa_n^{(0)}([T(\tilde{x})])\,\mathrm{d}\tilde{x}$$

$$\text{as } x_2 \to \infty \tag{4.4}$$

where

$$\Theta_n \equiv -\int_0^\infty \left[\frac{1}{2s^{*2}} + \frac{\mathrm{e}^{3\mathrm{i}\pi/4}\lambda^*}{\rho_n^{\frac{3}{2}}(\lambda^{*2}+1)}\right]\mathrm{d}\lambda^* \tag{4.5}$$

is a function of $\mu^*$ only, and the proper interpretation of the divergent integral

$$\int_{x_c}^{x} \kappa_n^{(0)}([T(x)])\,\mathrm{d}x$$

is

$$\mathrm{i}\int_{x_c}^{x} \kappa_n^{(0)}([T(x)])\,\mathrm{d}x \equiv \mathrm{e}^{3\mathrm{i}\pi/4}\left(\frac{S_0}{\rho_n}\right)^{\frac{3}{2}}\left[\int_{x_c}^{x}\left[\frac{1}{T(x)} - \frac{1}{\lambda_0'(x-x_c)}\right]\mathrm{d}x + \frac{1}{\lambda_0'}\ln(x-x_c)\right] \tag{4.6}$$

and $T(x) \equiv T(x, R)$ is defined by (3.4).

It follows from (4.4) and the requirements of matching with (2.85), that the eigensolution (3.8) will behave like

$$\tilde{u} \sim C_0^{(n)}\bar{a}_0(x)\,U' \exp\left[\frac{\mathrm{i}}{\epsilon^3}\int_{x_c}^{x} \kappa_n^{(0)}([T(\tilde{x})])\,\mathrm{d}\tilde{x}\right] \quad \text{for } x - x_c = O(1), \tag{4.7}$$

† We decided not to consider this scaling because our order of magnitude estimates show that, for fixed source frequency, Tollmien–Schlichting waves generated further downstream by the case (1) receptivity mechanism discussed in §1 will always have much larger amplitudes at the lower branch of the neutral stability curves, where they can begin to grow.

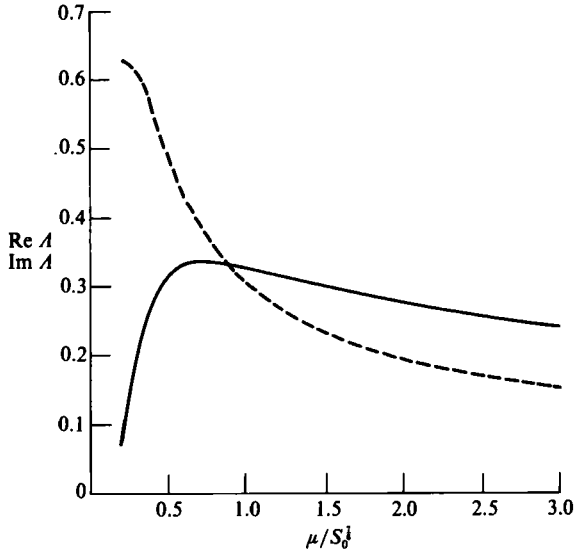


FIGURE 6. Real (——) and imaginary (– – – –) parts of $\Lambda$.

where

$$C_0^{(n)} \equiv \epsilon^2 \frac{\lambda_0'}{\mu S_0} \Lambda A^{\mathrm{T}}\left(\frac{\kappa_n}{\epsilon^{\frac{6}{5}}}\right) \exp\left\{\frac{S_0^{\frac{3}{2}}}{\epsilon^3 \lambda_0'}\left[\Theta_n + \left(\frac{e^{\frac{1}{2}i\pi}}{\rho_n}\right)^{\frac{3}{2}} \ln\left(\frac{\lambda_0' S_0^{\frac{1}{2}}}{\epsilon\mu}\right)\right]\right\} \tag{4.8}$$

is an effective 'coupling coefficient' that accounts for the net growth/decay of the instability wave in the intermediate region $x_2 = O(1)$. The first term in the exponent of the additional factor, being $O(\exp(\text{constant}/\epsilon^3))$, can more than compensate for the exponentially small factor in the Fourier transform $A^{\mathrm{T}}(\kappa_n/\epsilon^{\frac{6}{5}})$ of mean wall shear, which arises from the mismatch of its lengthscale with the instability wavelength. In a strict asymptotic sense this will of course be counteracted by the exponentially small $O(\exp[-\text{constant}\ (\ln 1/\epsilon)/\epsilon^3])$ term. But, since $\epsilon$ cannot, as we have already indicated, be very different from unity, the net result could augment the coupling coefficient numerically, if not in a strict asymptotic sense.

The $\Lambda$-factor depends only on the argument $\mu/S_0^{\frac{7}{6}}$ and is plotted as a function of that argument for the $n = 1$ mode in figure 6. $\bar{a}_0(x)$ is an $O(1)$ slowly varying amplitude function whose calculation is beyond the scope of this work.

Since $\kappa_n = O(1)$ and $T = O(1)$ in the region $x > x_c$, $x - x_c = O(1)$; it follows from (2.26), (2.85) and (4.7) that the disturbance wavelengths in this latter region are now formally much larger than their initial wavelengths, $\epsilon^4/\mathrm{Re}\,\kappa_n$, owing to the gradual relaxation of the strong adverse pressure gradient (which allows the wall shear to return to normal).

At the even larger downstream distances, where $T$ takes on the behaviour indicated in second expression (3.5),

$$\frac{\mathrm{i}}{\epsilon^3} \int_{x_c}^{x} \kappa_n^{(0)}([T])\,\mathrm{d}x \sim \left(\frac{SU_e}{\rho_n U_\infty}\right)^{\frac{3}{2}} e^{3i\pi/4} \frac{(2x)^{\frac{3}{2}}}{3\lambda_B} = \frac{e^{3i\pi/4}}{3\lambda_B}\left(\frac{2\omega x^*}{U_\infty \rho_n}\right)^{\frac{3}{2}} \quad \text{as } x \to \infty, \tag{4.9}$$

which shows that the wavelength is no longer increasing with increasing $x$ but is now decreasing like $x^{-\frac{1}{2}}$. In fact the eigensolutions (4.7) now coincide with the 'Lam & Rott' (1960) asymptotic eigensolutions of the unsteady boundary-layer equation appropriately corrected for the decaying external static pressure gradient. They

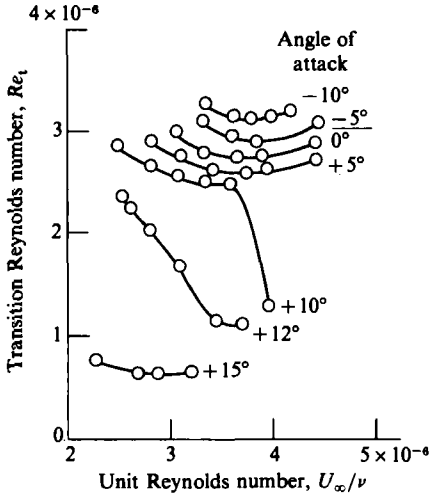


FIGURE 7. Effect of angle of attack on transition Reynolds number (data of Polyakov 1973*a*, *b*).

therefore turn into decaying Tollmien–Schlichting waves by the wavelength reduction mechanism described by Goldstein (1983). The lowest-order root $\rho_1$ evolves into the Tollmien–Schlichting wave that ultimately exhibits spatial growth in the downstream region. We therefore conclude that *the spatially growing Tollmien–Schlichting wave evolves from the eigenmode that originally exhibited spatial growth in the intermediate region* $x_2 = O(1)$ (see figure 2).

While we are unable to make direct quantitative comparisons with any of the experiments of which we are aware, the theory does provide qualitative explanations of a number of observed phenomena. The effects of angle of attack on flat-plate boundary-layer transition were studied by Polyakov (1973*a*, *b*). His measurements (reproduced here as figure 7) show that the transition Reynolds number $Re_t$ is strongly dependent on the angle of attack, and an analysis of the results shows that the changes in angle of attack had very little effect on the pressure gradients near the lower branch of the neutral stability curve but produced very steep adverse pressure gradients near the leading edge. Since the latter probably produced significant decreases in the wall shear, the observed decrease in $Re_t$ may be attributable to the receptivity mechanism considered in this paper. Vorob'yev *et al.* (1976) conducted similar experiments but used a small trailing-edge flap to generate their adverse pressure gradients. Their results are similar to those of Polyakov (1973*a*, *b*). Figure 8 shows their measured static pressures at various flap angles. Curves 3–6 probably correspond to marginally separated flows.

Another relevant experiment was conducted by Kachanov, Kozlov & Levchenko (1978), who produced their unsteady flow by placing a vibrating ribbon somewhat below and at an unspecified distance upstream of the leading edge of their flat plate. They measured the unsteady velocity fluctuations in the upper surface boundary layer and found that they exhibited a large peak just downstream of the maximum mean flow velocity and a very rapid downstream decay beyond that point. Their data are shown in figure 9. The relatively large maximum in the mean surface velocity suggests that their plate was at an angle of attack to the stream and that the flow was marginally separated. The peak in the velocity fluctuations may therefore be associated with a local instability of that flow. The rapid downstream decay would

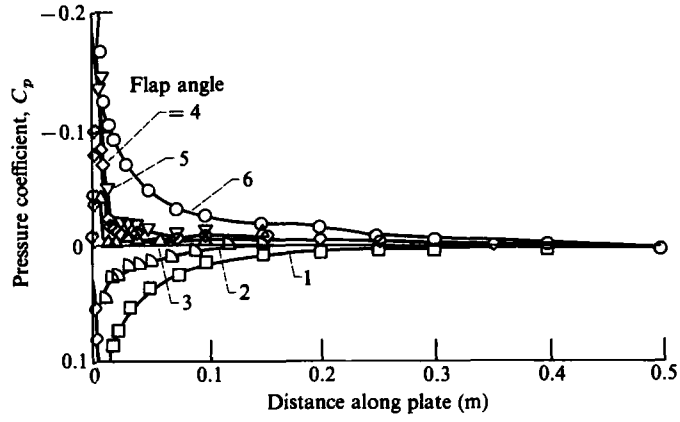


FIGURE 8. Static pressure distribution for various flap angles in Vorob'yev *et al.* (1976) experiment.

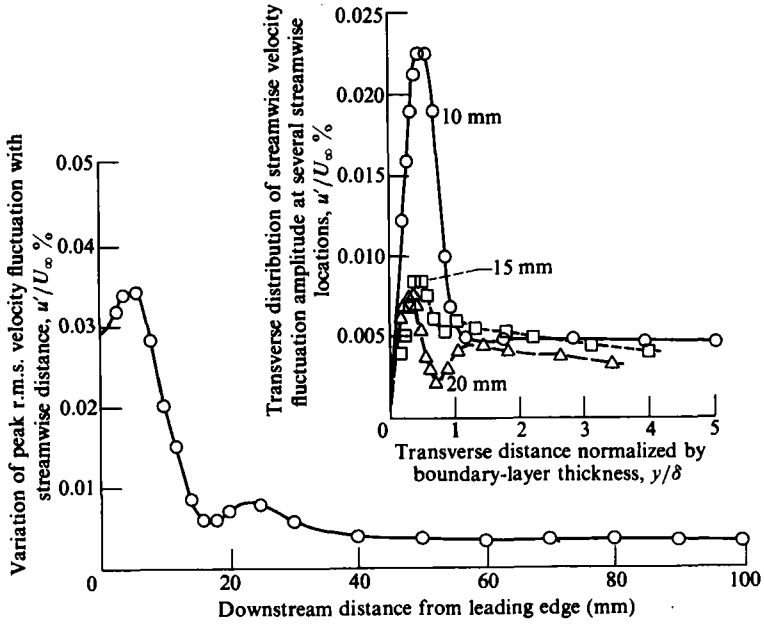


FIGURE 9. R.m.s. velocity fluctuation measured by Kachanov *et al.* (1978) (also containing data left out of paper, supplied by Professor M. V. Morkovin).

then be attributable to the stabilization of the boundary layer resulting from the subsequent increase in wall shear.

Paterson *et al.* (1972) and Arbey & Bataille (1983) studied the tones produced by an airfoil in a completely uniform and presumably steady mean flow. Fink (1975) suggested that they could be attributed to a feedback mechanism involving upstream-propagating acoustic disturbances generated by Tollmien–Schlichting waves passing over the trailing edge. The process would be self-sustaining if the acoustic waves were able to regenerate the Tollmien–Schlichting waves at some point in the laminar boundary layer, which Arbey & Bataille (1983) found to be the maximum-thickness

point. Smith (1986) suggests that marginally separated flows occur just downstream of the maximum-thickness point on thick airfoils such as those used in these experiments. We therefore expect the present receptivity mechanism to have played a role in producing the tones that were observed there.

The authors would like to thank Professor F. T. Smith (University College, London) for sending one of them (M.E.G.) an earlier version of his paper with Elliott on dynamic stall, Professor M. V. Morkovin for providing some data left out of Kachanov, Kozlov & Levchenko (1978), and Mr David Wundrow for helping with the numerical computations. S.J.C. is grateful to Professor D. W. Moore for helpful discussions of the work.

## Appendix A

Since the dispersion relation (3.28) determines $\kappa$ as a function of $\lambda$ (for a given $S_0$ and $\mu$), it follows from (3.3)–(3.6) and (3.39) that

$$\kappa_c \sim \kappa([\lambda_0' x_2]) + \kappa^{(\infty)}\left(\left[\frac{T}{\epsilon}\right]\right) - \kappa^{(\infty)}([\lambda_0' x_2]), \tag{A 1}$$

where

$$\kappa^{(\infty)}([\lambda]) \equiv \frac{e^{3i\pi/4}}{i}\left(\frac{S_0}{\rho_n}\right)^{\frac{3}{2}} \frac{\lambda}{\lambda^2 + (\mu^2/S_0)} \tag{A 2}$$

is (to lowest order of approximation) a uniformly valid composite expansion of the complete wavenumber $\kappa_c$ in $0 \leqslant x - x_c \ll \epsilon^{-1}$ as $\epsilon \to 0$. It therefore follows that

$$\begin{aligned} i\int_0^X \kappa_c \, dX &= i\int_0^\infty \{\kappa([\lambda_0' x_2]) - \kappa^{(\infty)}([\lambda_0' x_2])\} \, dX \\ &\quad - i\int_X^\infty \{\kappa([\lambda_0' x_2]) - \kappa^{(\infty)}([\lambda_0' x_2])\} \, dX + i\int_0^X \kappa^{(\infty)}\left(\left[\frac{T}{\epsilon}\right]\right) dX \\ &\approx i\int_0^\infty \{\kappa([\lambda_0' x_2]) - \kappa^{(\infty)}([\lambda_0' x_2])\} \, dX + i\int_0^X \kappa^{(\infty)}\left(\left[\frac{T}{\epsilon}\right]\right) dX \quad \text{for } x_2 \gg 1; \end{aligned} \tag{A 3}$$

then since

$$\kappa^{(\infty)}\left(\left[\frac{T}{\epsilon}\right]\right) \sim \frac{e^{3i\pi/4}}{i}\left(\frac{S_0}{\rho_n}\right)^{\frac{3}{2}}\left\{\frac{\lambda_0' x_2}{(\lambda_0' x_2)^2 + (\mu^2/S_0)} + \epsilon\left[\frac{1}{T(x)} - \frac{1}{\lambda_0'(x - x_c)}\right]\right\} \tag{A 4}$$

is a uniformly valid leading-order composite expansion for $\kappa^{(\infty)}([T/\epsilon])$ in $x_c \leqslant x \leqslant \infty$ as $\epsilon \to 0$, it follows from (3.28), (3.29), (3.21), (4.1) and (4.2) that (A 3) can be put in the form (4.3).

## Appendix B. Asymptotic expansion of dispersion relation

In this Appendix we derive a formula for the asymptotic expansion of the derivative of the parabolic cylinder function in terms of the Airy-function derivative Ai′.

It follows from Olver (1959, equations (4.14), (4.16), (7.4), (8.13), (8.15), (8.16) and (8.19)) that

$$U'\left(-\frac{\mu_0^2}{2}, \mu_0 t\sqrt{2}\right) \sim (2\pi)^{\frac{1}{2}} \mu_0^{\frac{3}{2}} g(\mu_0)\left(\frac{t^2 - 1}{\xi_0}\right)^{\frac{1}{4}} \mathrm{Ai}'(\mu_0^{\frac{4}{3}} \xi_0) \tag{B 1}$$

as $|\mu_0| \to \infty$, $-\pi < \arg \mu_0 < \pi$, uniformly with respect to $t$, with $t$ restricted to the domain depicted in Olver (1959, figure 7), $g(\mu_0)$ denoting a function of $\mu_0$ whose asymptotic expansion is given by Olver (1959, equation (6.2)) and

$$\tfrac{2}{3}\xi_0^{\frac{3}{2}} \equiv \int_1^t (t^2-1)^{\frac{1}{2}}\,\mathrm{d}t. \tag{B 2}$$

Then

$$\xi_0 \approx 2^{\frac{1}{3}}(t-1) \tag{B 3}$$

for $|t-1| \ll 1$, and (B 1) becomes

$$U'\left(-\frac{\mu_0^2}{2}, \mu_0 t\sqrt{2}\right) \sim g_0(\mu_0)\,\mathrm{Ai}'\left((2\mu_0^4)^{\frac{1}{3}}(t-1)\right) \quad \text{for } |t-1| \ll 1, \tag{B 4}$$

where we have put

$$g_0(\mu_0) \equiv (2\pi)^{\frac{1}{2}} 2^{\frac{1}{6}} \mu_0^{\frac{3}{2}} g(\mu_0).$$

## Appendix C

This Appendix further explains the choice of streamwise lengthscale, say $l\delta$, normalized forcing frequency, i.e. Strouhal number $S$, and minimum wall-shear $\tau_{\min}$, that was adopted in §2. Figure 10 is a summary of the Reynolds-number scaling, in the limit $R \to \infty$, of the (asymptotically distinct) discrete normal modes of given real Strouhal number that can exist on a mean boundary-layer flow with scaled wall shear $T$ and normalized inviscid pressure gradient $\mu$ (see (3.2)–(3.4) for the definition of $T$, and recall that $\mu$ is assumed to be positive and order one). There is a unique relation between the orders of magnitude of $S$, $T$ and $\delta$ for any given mode, and for simplicity we choose to explicitly exhibit the relation between the first two.

We begin with the long dashed line, which corresponds to an unsteady triple-deck interaction scaling for the case where the mean velocity in the viscous wall layer is dominated by the pressure-gradient term $\frac{1}{2}\mu y^2$ rather than the wall-shear term $Ty$.

This is the scaling that was used in §2. It also applies at the intersection point A where the wall-shear and pressure-gradient terms of the mean velocity are of the same order in the lower deck. The point A therefore corresponds to the scaling $T = O(R^{-\frac{1}{14}})$, which is indicated in figure 10 and which was used in §3 to study the eigenmodes in the outer region (i.e. region 2 in figure 2). This scaling produces the most general eigenmode structure consistent with the triple-deck interaction. The solid line extending to the right of point A corresponds to the standard unsteady triple-deck interaction scaling $S = O(R^{\frac{1}{4}}T^{\frac{9}{4}})$, which applies in the vicinity of the lower branch of the neutral stability curve (Reid 1965; Smith 1979; Goldstein 1983).

The eigenmodes are generated by variations in the wall shear $T$, and these variations are most rapid where $T$ is a minimum. A scaling with $S = O(R^{\frac{1}{7}})$ and $\tau_{\min} = O(R^{-\frac{1}{14}})$ would therefore seem of interest, because the most general type of eigenmode would be excited in the region of marginal separation. However, the steady flow is non-interactive and an analysis analogous to that in §2 for this scaling leads to a governing equation that is not easy to solve by, for instance, a Green-function technique (the equation is related to (3.15)). Moreover, point B corresponds to the shortest mean flow lengthscale and therefore leads to the best match between the steady- and unsteady-flow streamwise lengthscales and consequently to the largest coupling coefficient. We therefore chose to study the scaling marked by point B in figure 10, i.e. $S = O(R^{\frac{1}{7}})$ and $\tau_{\min} = O(R^{-\frac{1}{8}})$, which combines an interactive steady flow with a general form of eigenmode in the region of marginal separation.

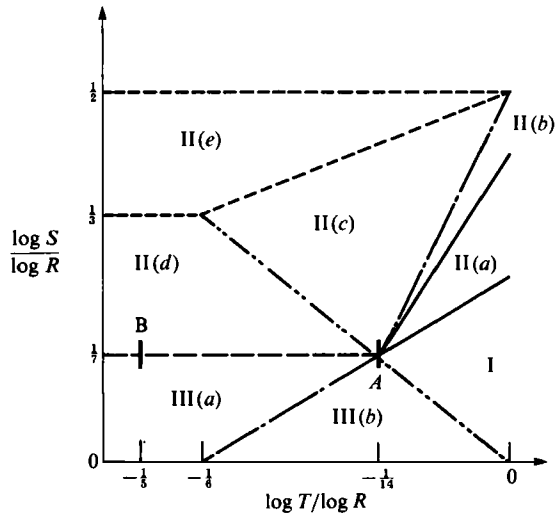


FIGURE 10. Parameter space for discrete normal modes, $\mu > 0$. (i) The $n = 1$ mode. Region I: non-interactive decaying mode. Region II($a$): growing Tollmien–Schlichting wave. Regions II($b$–$e$): long-wavelength growing Rayleigh mode. Region III($a$): interactive growing Ruban–Ryzhov–Smith mode. Region III($b$): non-interactive decaying Smith–Elliott mode. Regions I, II($a, b$): wall-shear component of mean flow dominant in lower layer. Regions II($c$–$e$), III($a, b$): pressure-gradient component of mean flow dominant in lower layer. (ii) The $n = 2, 3, 4, \ldots$ decaying modes. Regions I, III: non-interactive asymptotic structure. Regions II($a$–$d$): zero-displacement asymptotic structure. Regions I, II($a$–$c$): wall-shear component of mean flow dominant in lower viscous layer. Regions II($d$), III: pressure-gradient component of mean flow dominant in lower viscous layer. (iii) Range of validity in parameter space of limiting forms of the coupling coefficient (4.8) (abscissa $\log \tau_{\min}/\log R$). $n = 1$ mode: regions II($c$–$e$) and III($a$). $n = 2, 3, \ldots$ modes: region II($d$) (possibly regions III($a, b$), but further analysis required).

Only Lam & Rott (1960) eigenmodes can exist in region I. There are an 'infinite' number of these non-interactive modes, all of which decay in the downstream direction as a result of viscous effects. There are also infinitely many spatially decaying eigenmodes in regions II ($a$–$d$) and III. In region III, they have a non-interactive asymptotic structure, with fluctuations in displacement that are much larger than those in pressure gradient; and vice versa in regions II ($a$–$d$). The largest contribution to the lower-deck mean flow velocity comes from the wall-shear term in the regions to the right of the dash/double-dot line, and from the pressure-gradient term in the regions to the left. (The dividing scaling is obtained by equating the temporal and viscous terms in (2.34) to determine the wall-layer thickness, and then equating the wall-shear and pressure-gradient terms in the corresponding mean-flow velocity.) At the boundary between regions II ($c, d$) and II ($e$) these decaying modes are governed by the linearized Navier–Stokes equations and there are pressure variations across the main deck.

In addition to the decaying modes, there is also at least one growing mode in region II. In region II ($a$), the growing mode is a Tollmien–Schlichting wave and viscous effects determine its growth rate (the upper solid line is the scaling at which the upper branch of the neutral curve would be found if $\mu < 0$, cf. Reid 1965). The boundary-layer-thickness Strouhal number is order one on the uppermost dotted line, which means that the mode is unsteady over the entire boundary layer along this line, and

of relatively low frequency and long wavelength below it. Hence in regions II (*b–e*) the growing eigenmode is essentially a long-wavelength inviscid Rayleigh mode (recall that the mean flow is inflexional because the pressure gradient $\mu$ is assumed to be positive). The asymptotic structure in regions II (*b*)/II (*c–e*) is slightly different because respectively the wall-shear/pressure-gradient terms of the mean flow dominate in a thin inviscid layer close to the wall.

In region III there is also a mode with a unique asymptotic structure. It can be deduced as a 'high'-frequency limiting case of the viscous low-frequency mode studied by Ruban (1982*b*), and Ryzhov & Smith (1984) for $S \sim R^{-\frac{1}{10}}$. This mode is interactive and growing in region III (*a*), and non-interactive and decaying in III (*b*) (Smith & Elliott 1985).

Since the scaling we have chosen is unlikely to agree precisely with experimental conditions, it is important to assess the region of parameter space for which our formula (4.8) for the coupling coefficient remains valid. If the abscissa of figure 10 is taken as $\log \tau_{\min}/\log R$, then a limiting form of (4.8) is valid in regions II (*c–e*) for the growing $n = 1$ mode, and in region II (*d*) for the decaying $n = 2, 3, \ldots$ modes. It has to be modified along the dot/dash and double-dot/dash lines respectively, to account for the fact that the pressure-gradient and wall-shear terms of the mean flow are of equal magnitude in the wall layer there.

Formula (4.8) can also be extended into region III (*a*) for the $n = 1$ mode, and possibly into regions III (*a, b*) for the $n = 2, 3, 4, \ldots$ modes. In the latter case, the analysis is complicated by the fact that the real part of the roots $\kappa_n$ for $n = 2, 3, 4, \ldots$ tends to zero in the inner region 1 of figure 2. The resulting lower-deck asymptotic formulas for the corresponding, non-interactive modes, which are valid when $Y = O(1)$, (where $Y$ is defined in (2.30)) do not give decay as $Y \to \infty$, which makes matching with the main-deck solution impossible. These modes can then only exist in some limiting asymptotic sense.

## REFERENCES


Abramowitz, M. & Stegun, I. A. 1964 *Handbook of Mathematical Functions.* National Bureau of Standards.

Ackerberg, R. C. & Phillips, J. H. 1972 The unsteady laminar boundary layer on a semi-infinite flat plate due to small fluctuations in the magnitude of the free-stream velocity. *J. Fluid Mech.* **51**, 137–157.

Arbey, H. & Bataille, J. 1983 Noise generated by airfoil profiles placed in a uniform laminar flow. *J. Fluid Mech.* **134**, 33–47.

Bers, A. 1975 Linear waves and instabilities. In *Plasma Physics* (ed. C. DeWitt & J. Peyraud), pp. 113–216. Gordon & Breach.

Briggs, R. J. 1964 *Electron Stream Interaction With Plasmas.* Massachusetts Institute of Technology Press.

Carrier, G. F., Krook, M. & Pearson, C. E. 1966 *Functions of a Complex Variable.* McGraw-Hill.

Crighton, D. G. & Leppington, F. G. 1974 Radiation properties of the semi-infinite vortex sheet: the initial-value problem. *J. Fluid Mech.* **64**, 393–414.

Dingle, R. B. 1973 *Asymptotic Expansions: Their Derivation and Interpretation.* Academic.

Elliott, J. W. & Smith, F. T. 1987 Dynamic stall due to unsteady marginal separation. *J. Fluid Mech.* **179**, 489–512.

Fink, M. R. 1975 Prediction of airfoil tone frequencies. *J. Aircraft* **12**, 118–120.

Goldstein, M. E. 1983 The evolution of Tollmien–Schlichting waves near a leading edge. *J. Fluid Mech.* **127**, 59–81.

GOLDSTEIN, M. E. 1985 Scattering of acoustic waves into Tollmien–Schlichting waves by small streamwise variations in surface geometry. *J. Fluid Mech.* **154**, 509–529.

GOLDSTEIN, M. E., SOCKOL, P. M. & SANZ, J. 1983 The evolution of Tollmien–Schlichting waves near a leading edge. Part 2. Numerical determination of amplitudes. *J. Fluid Mech.* **129**, 443–453.

GOLDSTEIN, S. 1948 On laminar boundary layer flow near a position of separation. *Q. J. Mech. Appl. Maths* **1**, 43–69.

KACHANOV, Y. S., KOZLOV, V. V. & LEVCHENKO, V. Y. 1978 Occurrence of Tollmien–Schlichting waves in the boundary layer under the effect of external perturbations. *Fluid Dyn.* **13**, 704–711 (Engl. Transl.).

LAM, S. H. & ROTT, N. 1960 Theory of linearized time-dependent boundary layers. *AFOSR* TN 60–1100.

LIGHTHILL, M. J. 1954 The response of laminar skin friction and heat transfer to fluctuations in the stream velocity. *Proc. R. Soc. Lond.* A **224**, 1–23.

LYNE, W. H. 1970 Steady streaming associated with some unsteady viscous flows. Ph.D. thesis, Dept. of Mathematics, Imperial College of Science and Technology, London.

MORKOVIN, M. V. 1969 Critical evaluation of transition from laminar to turbulent shear layer with emphasis on hypersonically traveling bodies. *AFFDL-TR*-68-149.

MOORE, D. W. 1979 The spontaneous appearance of a singularity in the shape of an evolving vortex sheet. *Proc. R. Soc. Lond.* A **365**, 105–119.

MURDOCK, J. W. 1980 The generation of a Tollmien–Schlichting wave by a sound wave. *Proc. R. Soc. Lond.* A **372**, 517–534.

NAYFEH, A. H. 1973 *Perturbation Methods*. Wiley.

OLVER, F. W. J. 1959 Uniform asymptotic expansions for Weber parabolic cylinder functions of large orders. *J. Res. Natn. Bur. Stand.* B **63**, 131–169.

PATERSON, R. W., VOGT, P. G., FINK, M. R. & MUNCH, C. L. 1972 Vortex noise of isolated airfoils. *AIAA Paper* 72-656.

POLYAKOV, N. F. 1973*a* Method of study of flow characteristics in low turbulence wind tunnel and transition phenomena in an incompressible boundary layer. Candidate's dissertation, Institute of Theoretical and Applied Mechanics, Siberian Section USSR Academy of Sciences, Novosibirsk.

POLYAKOV, N. F. 1973*b* Aerophysical research, issue 2. *Sb. nauch. trudov* [Collected Scientific Works] p. 88. Institute of Theoretical and Applied Mechanics, Siberian Section USSR Academy of Sciences, Novosibirsk.

RESHOTKO, E. 1976 Boundary-layer stability and transition. In *Ann. Rev. Fluid Mech.* **8**, 311–349.

REID, W. H. 1965 The stability of parallel flows. In *Basic Developments in Fluid Mechanics*, Vol. 1 (ed. M. Holt), pp. 249–307. Academic.

RUBAN, A. I. 1982*a* Asymptotic theory of short separation regions on the leading edge of a slender airfoil. *Fluid Dyn.* **17**, 33–41 (Engl. Transl.).

RUBAN, A. I. 1982*b* Stability of preseparation boundary layer on the leading edge of a thin airfoil. *Fluid Dyn.* **17**, 860–867 (Engl. Transl.).

RUBAN, A. I. 1985 On the generation of Tollmien–Schlichting waves by sound. *Fluid Dyn.* **19**, 709–716 (Engl. Transl.).

RYZHOV, O. S. & SMITH, F. T. 1984 Short-length instabilities, breakdown and initial value problems in dynamic stall. *Mathematika* **31**, 163–177.

SMITH, F. T. 1979 On the non-parallel flow stability of the Blasius boundary layer. *Proc. R. Soc. Lond.* A **336**, 91–109.

SMITH, F. T. 1982 Concerning dynamic stall. *Aero. Q.* **33**, 331–352.

SMITH, F. T. 1986 Steady and unsteady boundary-layer separation. In *Ann. Rev. Fluid Mech.* **18**, 197–220.

SMITH, F. T. & ELLIOT, J. W. 1985 On the abrupt turbulent reattachment downstream of a leading edge separation. *Proc. R. Soc. Lond.* A **399**, 25–55.

STEWARTSON, K. 1981 Marginally stable inviscid flows with critical layers. *IMA J. Appl. Maths* **27**, 133–175.

STEWARTSON, K., SMITH, F. T. & KAUPS, K. 1982 Marginal separation. *Stud. Appl. Maths* **67**, 45–61.

VAN DYKE, M. 1975 *Perturbation Methods in Fluid Mechanics*. Parabolic.

VOROB'YEV, N. F., POLYAKOV, N. F., SHASHKINA, G. N. & SHCHERBAKOV, V. A. 1976 Physical gasdynamics. *Sb. nauch. trudov* [Collected Scientific Works], p. 101. Institute of Theoretical and Applied Mechanics, Siberian Section USSR Academy of Sciences, Novosibirsk.